Abstracta

Ano XXII - N. 01

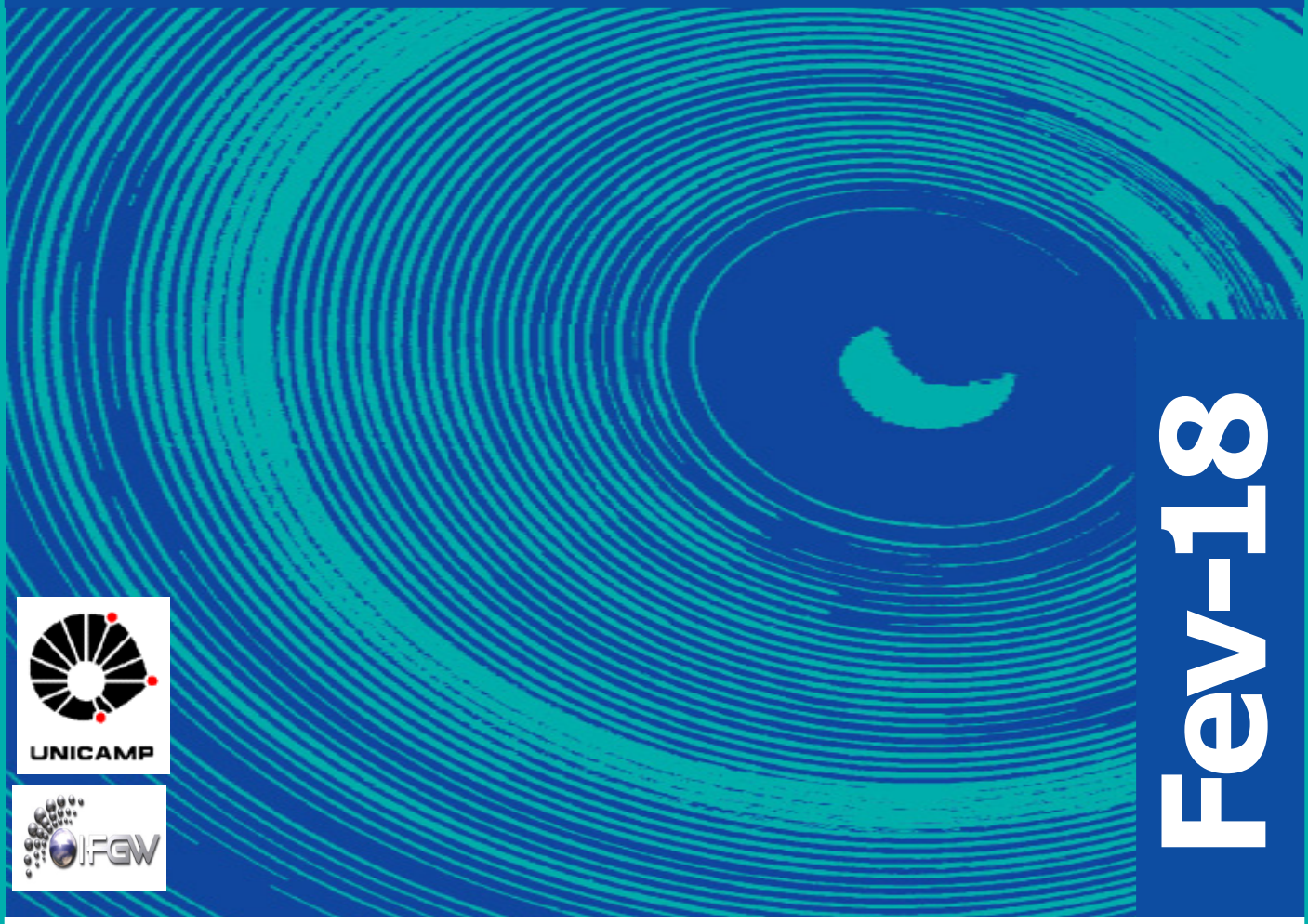

Fev-18

UNICAMP

IFGW

Artigos publicados 2017 - P327-2017 à P387-2017

Eventos publicados 2017 - P388-2017 à P391-2017

Artigos publicados 2018 - P001-2018 à P020-2018

Patentes 2017 - Pa005-2017 à Pa007-2017

Defesas de Dissertações do IFGW - D001-2018

Defesas de Teses do IFGW - T001-2018 à T005-2018

Artigos publicados 2017

[P327-2017] "Ab Initio Investigation of the Role of CO Adsorption on the Physical Properties of 55-Atom PtCo Nanoalloys"

Guedes-Sobrinho, D.; Freire, R. L. H.; **Chaves, A. S.***; Da Silva, J. L. F.

The knowledge of the physical and chemical properties of PtCo nanoparticles as a function of the Pt/Co composition and atomic distribution is crucial for several potential applications, which includes catalysis, anticorrosion, data storage, etc. However, our current atom-level understanding is far from satisfactory, in particular due to the challenges to take into account chemical environment effects. In this work, we report a density functional theory investigation of the structural, energetic, and electronic properties of binary 55-atom PtCo particles at a saturated CO atmosphere (31 molecules), (CO)(31)/Pt(n)Coss(55-n). For PtCo in the gas phase, which adopts an icosahedron-like (ICO-like) structure in the lowest-energy configurations for all studied compositions, we found a rough correlation between stability and the number of bonds among the Pt and Co species; i.e., the stability (excess energy) increases (decreases) by increasing the number of Pt and Co bonds and with a minimum at about n = 28-42 (Pt-rich). However, at a saturated CO atmosphere, we found a stability displacement toward higher Co concentration (n = 6-20, Co-rich), which can be explained by the structural expansion of the nanocluster surface driven by the CO ligands. That is, the CO adsorption contributes to release the strain, which is induced by the attractive Coulomb interactions between the anionic surface and cationic core regions. Furthermore, for particular compositions (n = 42), we found a displacement of the Co atoms toward the surface upon the CO adsorption, which can be explained also by strain release as the adsorption energy of CO is larger on the Pt surfaces, which could favor Pt-rich surfaces.

JOURNAL OF PHYSICAL CHEMISTRY C 121[49] 27721-27732, 2017. DOI: 10.1021/acs.jpcc.7b09243

[P328-2017] "Assisted laser ablation: silver/gold nanostructures coated with silica"

Gonzalez-Castillo, J. R.; Rodriguez-Gonzalez, E.; Jimenez-Villar, E.; **Cesar, C. L.***; Andrade-Arvizu, A. J.

The synthesis processes of metallic nanoparticles have seen a growing interest in recent years, mainly by the potential applications of the phenomenon of localized surface plasmon resonance associated with metallic nanoparticles. This paper shows a fast method to synthesize silver, gold and silver/gold alloy nanoparticles coated with a porous silica shell by the assisted laser ablation method in three steps. The method involves a redox chemical reaction where the reducing agent is supplied in nanometric form by laser ablation. In the first step, a silicon target immersed in water is ablated for several minutes. Later, AgNO3 and HAuCl4 aliquots are added to the solution. The redox reaction between the silver and gold ions and products resulting from ablation process can produce silver, gold or silver/gold alloy nanoparticles coated with a porous silica shell. The influence of the laser pulse energy, ablation time, Ag+ and Au3+ concentration, as well as the Ag+/Au3+ ratio, on optical and structural properties of the nanostructures was investigated. This work represents a step forward in the study of reaction mechanisms that take place during the synthesis of nanoscale materials by the assisted laser ablation technique.

APPLIED NANOSCIENCE 7[8], 597-605, 2017. DOI: 10.1007/s13204-017-0599-2

[P329-2017] "CALIS - A CALibration Insertion System for the DarkSide-50 dark matter search experiment"

Agnes, P.; Albuquerque, I. F. M.; Alexander, T.; **Segreto, E.***; et al.
DarkSide Collaboration

This paper describes the design, fabrication, commissioning and use of a CALibration source Insertion System (CALIS) in the DarkSide-50 direct dark matter search experiment. CALIS deploys radioactive sources into the liquid scintillator veto to characterize the detector response and detection efficiency of the DarkSide-50 Liquid Argon Time Projection Chamber, and the surrounding 30 t organic liquid scintillator neutron veto. It was commissioned in September 2014 and has been used successfully in several gamma and neutron source campaigns since then. A description of the hardware and an excerpt of calibration analysis results are given below.

JOURNAL OF INSTRUMENTATION 12, T12004, 2017. DOI: 10.1088/1748-0221/12/12/T12004

[P330-2017] "Charge carrier transport in defective reduced graphene oxide as quantum dots and nanoplatelets in multilayer films"

Jimenez, M. J. M.*; Oliveira, R. F.; Almeida, T. P.; **Hensel Ferreira, R. C.***; Bufon, C. C. B.; **Rodrigues, V.***; Pereira-da-Silva, M. A.; Gobbi, A. L.; Piazzetta, M. H. O.; **Riul, A.***

Graphene is a breakthrough 2D material due to its unique mechanical, electrical, and thermal properties, with considerable responsiveness in real applications. However, the coverage of large areas with pristine graphene is a challenge and graphene derivatives have been alternatively exploited to produce hybrid and composite materials that allow for new developments, considering also the handling of large areas using distinct methodologies. For electronic applications there is significant interest in the investigation of the electrical properties of graphene derivatives and related composites to determine whether the characteristic 2D charge transport of pristine graphene is preserved. Here, we report a systematic study of the charge transport mechanisms of reduced graphene oxide chemically functionalized with sodium polystyrene sulfonate (PSS), named as GPSS. GPSS was produced either as quantum dots (QDs) or nanoplatelets (NPLs), being further nanostructured with poly(diallyldimethylammonium chloride) through the layer-by-layer (LbL) assembly to produce graphene nanocomposites with molecular level control. Current-voltage (I-V) measurements indicated a meticulous growth of the LbL nanostructures onto gold interdigitated electrodes (IDEs), with a space-charge-limited current dominated by a Mott-variable range hopping mechanism. A 2D intra-planar conduction within the GPSS nanostructure was observed, which resulted in effective charge carrier mobility (mu) of 4.7 cm(2) V-1 s(-1) for the QDs and 34.7 cm(2) V-1 s(-1) for the NPLs. The LbL assemblies together with the dimension of the materials (QDs or NPLs) were favorably used for the fine tuning and control of the charge carrier mobility inside the LbL nanostructures. Such 2D charge conduction mechanism and high ae values inside an interlocked multilayered assembly containing graphene-based nanocomposites are of great interest for organic devices and functionalization of interfaces.

NANOTECHNOLOGY 28[49], 495711, 2017. DOI: 10.1088/1361-6528/aa91c2

[P331-2017] "Charged-particle multiplicity distributions over a wide pseudorapidity range in proton-proton collisions at root s=0.9, 7, and 8 TeV"

Acharya, S.; Adamova, D.; Adolfsson, J; **Albuquerque, D. S. D.*; Chinellato, D. D.*; De Souza, R. D.*; Takahashi, J.***; et al.
ALICE Collaboration

We present the charged-particle multiplicity distributions over a wide pseudorapidity range (-3.4<eta<5.0) for pp collisions at root s = 0.9, 7, and 8 TeV at the LHC. Results are based on information from the Silicon Pixel Detector and the Forward Multiplicity Detector of ALICE, extending the pseudorapidity coverage of the earlier publications and the high--multiplicity reach. The measurements are compared to results from the CMS experiment and to PYTHIA, PHOJET and EPOS LHC event generators, as well as IP-Glasma calculations.

EUROPEAN PHYSICAL JOURNAL C 77[12], 852, 2017. DOI: 10.1140/epjc/s10052-017-5412-6

[P332-2017] "Combination of searches for heavy resonances decaying to WW, WZ, ZZ, WH, and ZH boson pairs in proton-proton collisions at root s=8 and 13 TeV"

Sirunyan, A. M.; Turnasyan, A.; Adam, W.; **Chinellato, J. A.*; Tonelli Manganote, E. J.*;** et al.
CMS Collaboration

A statistical combination of searches is presented for massive resonances decaying to WW, WZ, ZZ, WH, and ZH boson pairs in proton-proton collision data collected by the CMS experiment at the LHC. The data were taken at centre-of-mass energies of 8 and 13TeV, corresponding to respective integrated luminosities of 19.7 and up to 2.7 fb(-1). The results are interpreted in the context of heavy vector triplet and singlet models that mimic properties of composite-Higgs models predicting W' and Z' bosons decaying to WZ, WW, WH, and ZH bosons. A model with a bulk graviton that decays into WW and ZZ is also considered. This is the first combined search for WW, WZ, WH, and ZH resonances and yields lower limits on masses at 95% confidence level for W' and Z' singlets at 2.3 TeV, and for a triplet at 2.4TeV. The limits on the production cross section of a narrow bulk graviton resonance with the curvature scale of the warped extra dimension (K)over-tilde = 0.5, in the mass range of 0.6 to 4.0TeV, are the most stringent published to date.

PHYSICS LETTERS B 774, 533-558, 2017. DOI: 10.1016/j.physletb.2017.09.083

[P333-2017] "Constraints on anomalous Higgs boson couplings using production and decay information in the four--lepton final state"

Sirunyan, A. M.; Turnasyan, A.; Adam, W.; **Chinellato, J. A.*; Tonelli Manganote, E. J.***; et al.
CMS Collaboration

A search is performed for anomalous interactions of the recently discovered Higgs boson using matrix element techniques with the information from its decay to four leptons and from associated Higgs boson production with two quark jets in either vector boson fusion or associated production with a vector boson. The data were recorded by the CMS experiment at the LHC at a center-of-mass energy of 13 TeV and correspond to an integrated luminosity of 38.6 fb(-1). They are combined with the data collected at center-of-mass energies of 7 and 8 TeV, corresponding to integrated luminosities of 5.1 and 19.7 fb(-1), respectively. All observations are consistent with the expectations for the standard model Higgs boson.

PHYSICS LETTERS B 775, 1-24, 2017. DOI: 10.1016/j.physletb.2017.10.021

[P334-2017] "Cornering the revamped BMV model with neutrino oscillation data"

Chatterjee, S. S.; Masud, M.; **Pasquini, P.***; Valle, J. W. F.

Using the latest global determination of neutrino oscillation parameters from [1] we examine the status of the simplest revamped version of the BMV (Babu-Ma-Valle) model, proposed in [2]. The model predicts a striking correlation between the "poorly determined" atmospheric angle 623 and CP phase Sep, leading to either maximal CP violation or none, depending on the preferred 623 octants. We determine the allowed BMV parameter regions and compare with the general three-neutrino oscillation scenario. We show that in the BMV model the higher octant is possible only at 99% C. L., a stronger rejection than found in the general case. By performing quantitative simulations of forthcoming DUNE and T2HK experiments, using only the four "well-measured" oscillation parameters and the indication for normal mass ordering, we also map out the potential of these experiments to corner the model. The resulting global sensitivities are given in a robust form, that holds irrespective of the true values of the oscillation parameters.

PHYSICS LETTERS B 774, 179-182, 2017. DOI: 10.1016/j.physletb.2017.09.052

[P335-2017] "Development of binary and ternary titanium alloys for dental implants"

Cordeiro, J. M.; Beline, T.; Ribeiroc, A. L. R.; Rangel, E. C.; da Cruz, N. C.; **Landers, R.***; Faverani, L. P.; Vaz, L. G.; Fais, L. M. G.; Vicente, F. B.; Grandini, C. R.; Mathew, M. T.; Sukotjo, C.; Barao, V. A. R.

Objective. The aim of this study was to develop binary and ternary titanium (Ti) alloys containing zirconium (Zr) and niobium (Nb) and to characterize them in terms of microstructural, mechanical, chemical, electrochemical, and biological properties. Methods. The experimental alloys - (in wt%) Ti-5Zr, Ti-10Zr, Ti--35Nb-5Zr, and Ti-35Nb-10Zr-were fabricated from pure metals. Commercially pure titanium (cpTi) and Ti-6Al-4V wereused as controls. Microstructural analysis was performed by means of X-ray diffraction and scanning electron microscopy. Vickers microhardness, elastic modulus, dispersive energy spectroscopy, X-ray excited photoelectron spectroscopy, atomic force microscopy, surface roughness, and surface free energy were evaluated. The electrochemical behavior analysis was conducted in a body fluid solution (pH 7.4). The albumin adsorption was measured by the bicinchoninic acid method. Data were evaluated through one-way ANOVA and the Tukey test (alpha = 0.05). Results. The alloying elements proved to modify the alloy microstructure and to enhance the mechanical properties, improving the hardness and decreasing the elastic modulus of the binary and ternary alloys, respectively. Ti-Zr alloys displayed greater electrochemical stability relative to that of controls, presenting higher polarization resistance and lower capacitance. The experimental alloys were not detrimental to albumin adsorption. Significance. The experimental alloys are suitable options for dental implant manufacturing, particularly the binary system, which showed a better combination of mechanical and electrochemical properties without the presence of toxic elements.

DENTAL MATERIALS 33[11], 1244-1257, 2017. DOI: 10.1016/j.dental.2017.07.013

[P336-2017] "Different growth regimes in InP nanowire growth mediated by Ag nanoparticles"

Oliveira, D. S.*; Zavarize, M.*; Tizei, L. H. G.; Walls, M.; Ospina, C. A.; **Iikawa, F.*; Ugarte, D.*; Cotta, M. A.***

We report on the existence of two different regimes in one-step Ag-seeded InP nanowire growth. The vapor-liquid-solid-mechanism is present at larger In precursor flows and temperatures, similar to 500 degrees C, yielding high aspect ratio and pure wurtzite InP nanowires with a semi-spherical metal particle at the thin apex. Periodic diameter oscillations can be achieved under extreme In supersaturations at this temperature range, showing the presence of a liquid catalyst. However, under lower temperatures and In precursor flows, large diameter InP nanowires with mixed wurtzite/zincblende segments are obtained, similarly to In-assisted growth. Chemical composition analysis suggest that In-rich droplet formation is catalyzed at the substrate surface via Ag nanoparticles; this process might be facilitated by the sulfur contamination detected in these nanoparticles. Furthermore, part of the original Ag nanoparticle remains solid and is embedded inside the actual catalyst, providing an in situ method to switch growth mechanisms upon changing In precursor flow. Nevertheless, our Ag-seeded InP nanowires exhibit overall optical emission spectra consistent with the observed structural properties and similar to Au--catalyzed InP nanowires. We thus show that Ag nanoparticles may be a suitable replacement for Au in InP nanowire growth.

NANOTECHNOLOGY 28[50], 505604, 2017. DOI: 10.1088/1361-6528/aa9816

[P337-2017] "Effective demagnetizing tensors in arrays of magnetic nanopillars"

Mendoza Zelis, P.; Vega, V.; Prida, V. M.; Costa-Arzuza, L. C.; **Beron, F.*; Pirota, K. R.*; Lopez-Ruiz, R.***; Sanchez, F. H.

A model describing the effect of magnetic dipolar interactions on the susceptibility of magnetic nanopillars is presented. It is an extension of a recently reported model for three-dimensional randomlike dispersions of nearly spherical nanoparticles in equilibrium [Sanchez et al., Phys. Rev. B 95, 134421 (2017)], to well-ordered arrays of nanoparticles out of equilibrium. To test it, a high-quality benchmark consisting of a two-dimensional hexagonal arrangement of quasi-identical parallel nickel nanopillars embedded in a porous alumina template was fabricated. This model is based on an effective demagnetizing tensor, which only depends on a few morphological parameters of the sample, as the nearest-neighbor distance between pillars and the volume fraction of pillars in the specimen. It allows us to obtain the nanopillar intrinsic susceptibility tensor from the magnetic response of the nanopillar ensemble. The values of the in-plane and normal-to-plane susceptibility of the sample are successfully predicted by the model. Furthermore, the model reproduces the susceptibility in the applied field direction, measured for different applied field angles. In this way, it provides a simple and accurate treatment to account for the complex magnetic effects produced by dipolar interactions.

PHYSICAL REVIEW B 96[17], 174427, 2017. DOI: 10.1103/PhysRevB.96.174427

[P338-2017] "Efficient anchor loss suppression in coupled near-field optomechanical resonators"

Luiz, G. O.*; Benevides, R. S.*; Santos, F. G. S.*; Espinel, Y. A. V.*; Alegre, T. P. M.*; Wiederhecker, G. S.*

Elastic dissipation through radiation towards the substrate is a major loss channel in micro-and nanomechanical resonators. Engineering the coupling of these resonators with optical cavities further complicates and constrains the design of low-loss optomechanical devices. In this work we rely on the coherent cancellation of mechanical radiation to demonstrate material and surface absorption limited silicon near-field optomechanical resonators oscillating at tens of MHz. The effectiveness of our dissipation suppression scheme is investigated at room and cryogenic temperatures. While at room temperature we can reach a maximum quality factor of 7.61k (fQ-product of the order of 10(11) Hz), at 22 K the quality factor increases to 37k, resulting in a fQ-product of 2 x 10(12) Hz.

OPTICS EXPRESS 25[25], 31347-31361, 2017. DOI: 10.1364/OE.25.031347

[P339-2017] "Elastic scattering and vibrational excitation for electron impact on&IT para&IT-benzoquinone"

Jones, D. B.; Blanco, F.; Garcia, G.; **da Costa, R. F.*; Kossoski, F.***; Varella, M. T. do N.; Bettega, M. H. F.; **Lima, M. A. P.***; White, R. D.; Brunger, M. J.

We report on theoretical elastic and experimental vibrational--excitation differential cross sections (DCSs) for electron scattering from para-benzoquinone (C6H4O2), in the intermediate energy range 15-50 eV. The calculations were conducted with two different theoretical methodologies, the Schwinger multichannel method with pseudopotentials (SMCPP) and the independent atom method with screening corrected additivity rule (IAM-SCAR) that also now incorporates a further interference (I) term. The SMCPP with N energetically open electronic states (N-open) at the static-exchange-plus-polarisation (N(open) ch-SEP) level was used to calculate the scattering amplitudes using a channel coupling scheme that ranges from 1ch-SE up to the 89ch-SEP level of approximation. We found that in going from the 38ch-SEP to the 89ch-SEP, at all energies considered here, the elastic DCSs did not change significantly in terms of both their shapes and magnitudes. This is a good indication that our SMCPP 89ch-SEP elastic DCSs are converged with respect to the multichannel coupling effect for the investigated intermediate energies. While agreement between our IAM--SCAR+I and SMCPP 89ch-SEP computations improves as the incident electron energy increases from 15 eV, overall the level of accord is only marginal. This is particularly true at middle scattering angles, suggesting that our SCAR and interference corrections are failing somewhat for this molecule below 50 eV. We also report experimental DCS results, using a crossed--beam apparatus, for excitation of some of the unresolved ("hybrid") vibrational quanta (bands I-III) of para-benzoquinone. Those data were derived from electron energy loss spectra that were measured over a scattered electron angular range of 10 degrees-90 degrees and put on an absolute scale using our elastic SMCPP 89ch-SEP DCS results. The energy resolution of our measurements was similar to 80 meV, which is why, at least in part, the observed vibrational features were only partially resolved. To the best of our knowledge, there are no other experimental or theoretical vibrational excitation results against which we might compare the present measurements.

JOURNAL OF CHEMICAL PHYSICS 147[24], 244304, 2017. DOI: 10.1063/1.5010831

[P340-2017] "Employing Calcination as a Facile Strategy to Reduce the Cytotoxicity in CoFe2O4 and NiFe2O4 Nanoparticles"

Lima, D. R.; Jiang, N.; Liu, X.; Wang, J.; Vulcani, V. A. S.; Martins, A.; Machado, D. S.; **Landers, R.***; Camargo, P. H. C.; Pancotti, A.

CoFe2O4 and NiFe2O4 nanoparticles (NPs) represent promising candidates for biomedical applications. However, in these systems, the knowledge over how various physical and chemical parameters influence their cytotoxicity remains limited. In this article, we investigated the effect of different calcination temperatures over cytotoxicity of CoFe2O4 and NiFe2O4 NPs, which were synthesized by a sol-gel proteic approach, toward L929 mouse fibroblastic cells. More specifically, we evaluated and compared CoFe2O4 and NiFe2O4 NPs presenting low crystallinity (that were calcined at 400 and 250 degrees C, respectively)

with their highly crystalline counterparts (that were calcined at 800 degrees C). We found that the increase in the calcination temperature led to the reduction in the concentration of surface defect sites and/or more Co or Ni atoms located at preferential crystalline sites in both cases. A reduction in the cytotoxicity toward mouse fibroblast L929 cells was observed after calcination at 800 degrees C. Combining with inductively coupled plasma mass spectrometry data, our results indicate that the calcination temperature can be employed as a facile strategy to reduce the cytotoxicity of CoFe2O4 and NiFe2O4, in which higher temperatures contributed to the decrease in the dissolution of Co2+ or Ni2+ from the NPs. We believe these results may shed new insights into the various parameters that influence cytotoxicity in ferrite NPs, which may pave the way for their widespread applications in biomedicine.

ACS APPLIED MATERIALS & INTERFACES 9[45], 39830-39838, 2017. DOI: 10.1021/acsami.7b13103

[P341-2017] "Exploring Au Droplet Motion in Nanowire Growth: A Simple Route toward Asymmetric GaP Morphologies"

da Silva, B. C.*; Oliveira, D. S.*; Iikawa, F.*; Couto, O. D. D.*; Bettini, J.; **Zagonel, L. F.*; Cotta, M. A.***

Here we show a new nanowire growth procedure, exploring the thermally activated motion of Au droplets on III-V surfaces. We show that by setting a single growth parameter we can activate the crawling motion of Au droplets in vacuum and locally modify surface composition in order to enhance vapor solid (VS) growth along oxide-free areas on the trail of the metal particle. Asymmetric VS growth rates are comparable in magnitude to the vapor liquid solid growth, producing unconventional wurtzite GaP morphologies, which shows negligible defect density as well as optical signal in the green spectral region. Finally, we demonstrate that this effect can also be explored in different substrate compositions and orientations with the final shape finely tuned by group III flow and nanoparticle size. This distinct morphology for wurtzite GaP nanomaterials can be interesting for the design of nanophotonics devices.

NANO LETTERS 17[12], 7274-7282, 2017. DOI: 10.1021/acs.nanolett.7b02770

[P342-2017] "Gap soliton transparency switching in one--dimensional Kerr-metamaterial superlattices"

Lobo, T. P.; **Oliveira, L. E.***; Cavalcanti, S. B.

Plasmon-polariton gap soliton formation and transparency switching in one-dimensional nonlinear layered systems composed of alternate layers of a Kerr material and a dispersive linear metamaterial are theoretically studied. The behavior of the electric field profile inside the layered system is shown for different values of nonlinear power, linking the localized modes of the electric field with complete transparency states of the system. A detailed investigation on the influence of a defocusing nonlinearity on the transmission switching phenomenon, in the frequency range where the linear dispersion predicts the photon-plasmon coupling, is made, revealing different effects in the top and bottom edges of the plasmon-polariton gap. Specifically, we found a broadening of the plasmon-polariton gap when increasing the nonlinear power. In addition, a switching from very low to high transmission states is obtained and localized plasmon-polariton gap solitons of various orders are found for various values of frequencies and nonlinear strength.

SUPERLATTICES AND MICROSTRUCTURES 112, 442-450, 2017. DOI: 10.1016/j.spmi.2017.09.052

[P343-2017] "Gas Adsorption and Separation by the Al-Based Metal-Organic Framework MIL-160"

Borges, D. D.*; Normand, P.; Permiakova, A.; Babarao, R.; Heymans, N.; **Galvao, D. S.***; Serre, C.; De Weireld, G.; Maurin, G.

One of the most promising technologies, with a low energy penalty, for CO2 capture from diverse gas mixtures is based on the adsorption process using adsorbents. Many efforts are still currently deployed to search for water stable porous metal--organic frameworks (MOFs) with high CO2 affinity combined with large CO2 uptake. In this context, we have selected the water stable and easily scalable Al-based MOF MIL-160 showing an ultramicroporosity and potential interacting sites (hydroxyl and furan), both features being a priori relevant to favor the selective adsorption of CO2 over other gases including H-2, N-2, CH4, and CO. Density functional theory (DFT) and force-field--based grand-canonical Monte Carlo (GCMC) simulations were first coupled to predict the strength of host/guest interactions and the adsorption isotherms for all guests as single components and binary mixtures. This computational approach reveals the promises of this solid for the selective adsorption of CO2 with respect to these other investigated gases, controlled by a combination of thermodynamics and confinement effects. These predicted performances were further supported by real-co-adsorption measurements performed on shaped samples which indicated that MIL-160(Al) shows promising performance for the selective CO2 capture in post- and pre-combustion conditions.

JOURNAL OF PHYSICAL CHEMISTRY C 121[48], 26822-26832, 2017. DOI: 10.1021/acs.jpcc.7b08856

[P344-2017] "Ground-State Properties of Unitary Bosons: From Clusters to Matter"

Carlson, J.; Gandolfi, S.; van Kolck, U.; **Vitiello, S. A.***

The properties of cold Bose gases at unitarity have been extensively investigated in the last few years both theoretically and experimentally. In this Letter we use a family of interactions tuned to two-body unitarity and very weak three-body binding to demonstrate the universal properties of both clusters and matter. We determine the universal properties of finite clusters up to 60 particles and, for the first time, explicitly demonstrate the saturation of energy and density with particle number and compare with bulk properties. At saturation in the bulk we determine the energy, density, two--and three-body contacts, and the condensate fraction. We find that uniform matter is more bound than three-body clusters by nearly 2 orders of magnitude, the two-body contact is very large in absolute terms, and yet the condensate fraction is also very large, greater than 90%. Equilibrium properties of these systems may be experimentally accessible through rapid quenching of weakly interacting boson superfluids.

PHYSICAL REVIEW LETTERS 119[22], 223002, 2017. DOI: 10.1103/PhysRevLett.119.223002

[P345-2017] "Inferences on mass composition and tests of hadronic interactions from 0.3 to 100 EeV using the water--Cherenkov detectors of the Pierre Auger Observatory"

Aab, A.; Abreu, P.; Aglietta, M.; **Chinellato, J. A.*; Daniel, B.*; Diaz Castro, M. L.*; Dobrigkeit, C.*; Fauth, A. C.*; Kemp, E.*; Muller, M. A.*; Pereira, L. A. S.*; Theodoro, V. M.***; et al.
Pierre Auger Collaboration

We present a new method for probing the hadronic interaction models at ultrahigh energy and extracting details about mass composition. This is done using the time profiles of the signals recorded with the water--Cherenkov detectors of the Pierre Auger Observatory.

The profiles arise from a mix of the muon and electromagnetic components of air showers. Using the risetimes of the recorded signals, we define a new parameter, which we use to compare our observations with predictions from simulations. We find, first, inconsistencies between our data and predictions over a greater energy range and with substantially more events than in previous studies. Second, by calibrating the new parameter with fluorescence measurements from observations made at the Auger Observatory, we can infer the depth of shower maximum X-max for a sample of over 81,000 events extending from 0.3 to over 100 EeV. Above 30 EeV, the sample is nearly 14 times larger than what is currently available from fluorescence measurements and extending the covered energy range by half a decade. The energy dependence of < X-max > is compared to simulations and interpreted in terms of the mean of the logarithmic mass. We find good agreement with previous work and extend the measurement of the mean depth of shower maximum to greater energies than before, reducing significantly the statistical uncertainty associated with the inferences about mass composition.

PHYSICAL REVIEW D 96[12], 122003, 2017. DOI: 10.1103/PhysRevD.96.122003

[P346-2017] "J/psi Elliptic Flow in Pb-Pb Collisions at root s(NN)=5.02 TeV"

Acharya, S.; Adamova, D.; Adolfsson, J.; **Albuquerque, D. S. D.*; Chinellato, D. D.*; De Souza, R. D.*; Takahashi, J.***; et al. ALICE Collaboration

We report a precise measurement of the J/psi elliptic flow in Pb-Pb collisions at root s(NN) = 5.02 TeV with the ALICE detector at the LHC. The J/psi mesons are reconstructed at midrapidity (|y| < 0.9) in the dielectron decay channel and at forward rapidity (2.5 < y < 4.0) in the dimuon channel, both down to zero transverse momentum. At forward rapidity, the elliptic flow v(2) of the J/psi is studied as a function of the transverse momentum and centrality. A positive v(2) is observed in the transverse momentum range 2<p(T)<8GeV/c in the three centrality classes studied and confirms with higher statistics our earlier results at root s(NN) = 2.76 TeV in semicentral collisions. At midrapidity, the J/psi v(2) is investigated as a function of the transverse momentum in semicentral collisions and found to be in agreement with the measurements at forward rapidity. These results are compared to transport model calculations. The comparison supports the idea that at low p(T) the elliptic flow of the J/psi originates from the thermalization of charm quarks in the deconfined medium but suggests that additional mechanisms might be missing in the models.

PHYSICAL REVIEW LETTERS 119[24], 242301, 2017. DOI: 10.1103/PhysRevLett.119.242301

[P347-2017] "Kaon femtoscopy in Pb-Pb collisions at root s(NN)=2.76 TeV"

Acharya, S.; Adam, J.; Adamova, D.; **Albuquerque, D. S. D.*; Chinellato, D. D.*; De Souza, R. D.*; Takahashi, J.***; et al. ALICE Collaboration

We present the results of three-dimensional femtoscopic analyses for charged and neutral kaons recorded by ALICE in Pb-Pb collisions at root s(NN) = 2.76 TeV. Femtoscopy is used to measure the space-time characteristics of particle production from the effects of quantum statistics and final--state interactions in two-particle correlations. Kaon femtoscopy is an important supplement to that of pions because it allows one to distinguish between different model scenarios working equally well for pions. In particular, we compare the measured three-dimensional kaon radii with a purely hydrodynamical calculation and a model where the hydrodynamic phase is followed by a hadronic rescattering stage. The former predicts an approximate transverse mass (m(T)) scaling of source radii obtained from pion and kaon correlations. This m(T) scaling appears to be broken in our data, which indicates the importance of the hadronic rescattering phase at LHC energies. A k(T) scaling of pion and kaon source radii is observed instead. The time of maximal emission of the system is estimated by using the three--dimensional femtoscopic analysis for kaons. The measured emission time is larger than that of pions. Our observation is well supported by the hydrokinetic model predictions.

PHYSICAL REVIEW C 96[6], 064613, 2017. DOI: 10.1103/PhysRevC.96.064613

[P348-2017] "Kelvin-Helmholtz instability of the Dirac fluid of charge carriers on graphene"

Coelho, R. C. V.; Mendoza, M.; **Doria, M. M.***; Herrmann, H. J.

We provide numerical evidence that a Kelvin-Helmholtz instability occurs in the Dirac fluid of electrons in graphene and can be detected in current experiments. This instability appears for electrons in the viscous regime passing though a micrometer-scale obstacle and affects measurements on the time scale of nanoseconds. A possible realization with a needle--shaped obstacle is proposed to produce and detect this instability by measuring the electric potential difference between contact points located before and after the obstacle. We also show that, for our setup, the Kelvin-Helmholtz instability leads to the formation of whirlpools similar to the ones reported in Bandurin et al. [Science 351, 1055 (2016)]. To perform the simulations, we develop a lattice Boltzmann method able to recover the full dissipation in a fluid of massless particles.

PHYSICAL REVIEW B 96[18], 184307, DOI: 10.1103/PhysRevB.96.184307

[P349-2017] "Leading components in forward elastic hadron scattering: Derivative dispersion relations and asymptotic uniqueness"

Fagundes, D. A.; **Menon, M. J.*; Silva, P. V. R. G.***

Forward amplitude analyses constitute an important approach in the investigation of the energy dependence of the total hadronic cross-section sigma(tot) and the rho parameter. The standard picture indicates for sigma(tot) a leading log-squared dependence at the highest c.m. energies, in accordance with the Froissart-Lukaszuk-Martin bound and as predicted by the COMPETE Collaboration in 2002. Beyond this log-squared (L2) leading dependence, other amplitude analyses have considered a log-raised-to-gamma form (L gamma), with gamma as a real free fit parameter. In this case, analytic connections with rho can be obtained either through dispersion relations (derivative forms), or asymptotic uniqueness (Phragmen-Lindeloff theorems). In this work, we present a detailed discussion on the similarities and mainly the differences between the Derivative Dispersion Relation (DDR) and Asymptotic Uniqueness (AU) approaches and results, with focus on the L gamma and L2 leading terms. We also develop new Regge-Gribov fits with updated dataset on sigma(tot) and rho from pp and (p) over barp scattering, including all available data in the region 5 GeV-8 TeV. The recent tension between the TOTEM and ATLAS results at 7 TeV and mainly at 8 TeV is discussed and considered in the data reductions. Our main conclusions are the following: (1) all fit results present agreement with the experimental data analyzed and the goodness-of-fit is slightly better in case of the DDR approach; (2) by considering only the TOTEM data at the LHC region, the fits with L gamma indicate gamma similar to 2.0 +/- 0.2 (AU approach) and gamma similar to 2.3 +/- 0.1 (DDR approach); (3) by including the ATLAS data the fits provide gamma similar to 1.9 +/- 0.1 (AU) and gamma similar to 2.2 +/- 0.2 (DDR);

(4) in the formal and practical contexts, the DDR approach is more adequate for the energy interval investigated than the AU approach. A pedagogical and detailed review on the analytic results for sigma(tot) and rho from the Regge-Gribov, DDR and AU approaches is presented. Formal and practical aspects related to forward amplitude analyses are also critically discussed.

INTERNATIONAL JOURNAL OF MODERN PHYSICS A 32[32], 1750184, 2017. DOI: 10.1142/S0217751X17501846

[P350-2017] "Measurement of charged pion, kaon, and proton production in proton-proton collisions at root s=13 TeV"

Sirunyan, A. M.; Turnasyan, A.; Adam, W.; **Chinellato, J. A.*; Tonelli Manganote, E. J.***; et al.
CMS Collaboration

Transverse momentum spectra of charged pions, kaons, and protons are measured in proton-proton collisions at root s = 13 TeV with the CMS detector at the LHC. The particles, identified via their energy loss in the silicon tracker, are measured in the transverse momentum range of p(T) approximate to 0.1-1.7 GeV/c and rapidities vertical bar y vertical bar < 1. The pT spectra and integrated yields are compared to previous results at smaller ffiffiffiffi root s and to predictions of Monte Carlo event generators. The average pT increases with particle mass and charged particle multiplicity of the event. Comparisons with previous CMS results at root s = 0.9, 2.76, and 7 TeV show that the average pT and the ratios of hadron yields feature very similar dependences on the particle multiplicity in the event, independently of the center-of-mass energy of the pp collision.

PHYSICAL REVIEW D 96[11], 112003, 2017. DOI: 10.1103/PhysRevD.96.112003

[P351-2017] "Measurement of the B-+/- Meson Nuclear Modification Factor in Pb-Pb Collisions at root s(NN)=5.02 TeV"

Sirunyan, A. M.; Turnasyan, A.; Adam, W.; **Chinellato, J. A.*; Tonelli Manganote, E. J.***; et al.
CMS Collaboration

The differential production cross sections of B-+/- mesons are measured via the exclusive decay channels B-+/- -> J/psi K-+/- -> mu(+)mu K--(+/-) as a function of transverse momentum in pp and Pb-Pb collisions at a center-of-mass energy root s(NN) = 5.02 TeV per nucleon pair with the CMS detector at the LHC. The pp(Pb - Pb) data set used for this analysis corresponds to an integrated luminosity of 28.0 pb(-1) (351 mu b(-1)). The measurement is performed in the B-+/- meson transverse momentum range of 7 to 50 GeV/c, in the rapidity interval vertical bar y vertical bar < 2.4. In this kinematic range, a strong suppression of the production cross section by about a factor of 2 is observed in the Pb-Pb system in comparison to the expectation from pp reference data. These results are found to be roughly compatible with theoretical calculations incorporating beauty quark diffusion and energy loss in a quark-gluon plasma.

PHYSICAL REVIEW LETTERS 119[15], 152301, 2017. DOI: 10.1103/PhysRevLett.119.152301

[P352-2017] "Measurement of the transverse momentum spectrum of the Higgs boson produced in pp collisions at root s=8 TeV using H -> WW decays"

Khachatryan, V., Sirunyan, A. M., Tumasyan, A., **Chinellato, J. A.*; Tonelli Manganote, E. J.***; et al.
Collaboration, CMS

The cross section for Higgs boson production in pp collisions is studied using the H -> W+ W- decay mode, followed by leptonic decays of the W bosons to an oppositely charged electron-muon pair in the final state. The measurements are performed using data collected by the CMS experiment at the LHC at a centre -of -mass energy of 8 TeV, corresponding to an integrated luminosity of 19.4 fb(-1). The Higgs boson transverse momentum (p(T)) is reconstructed using the lepton pair p(T), and missing p(T). The differential cross section times branching fraction is measured as a function of the Higgs boson p(T), in a fiducial phase space defined to match the experimental acceptance in terms of the lepton kinematics and event topology. The production cross section times branching fraction in the fiducial phase space is measured to be 39 +/- 8 (stat) +/- 9 (syst) fb. The measurements are found to agree, within experimental uncertainties, with theoretical calculations based on the standard model.

JOURNAL OF HIGH ENERGY PHYSICS [3], 032, 2017. DOI: 10.1007/JHEP03(2017)032

[P353-2017] "Measurement of vector boson scattering and constraints on anomalous quartic couplings from events with four leptons and two jets in proton-proton collisions at root s=13 TeV"

Sirunyan, A. M.; Turnasyan, A.; Adam, W.; **Chinellato, J. A.*; Tonelli Manganote, E. J.***; et al.
CMS Collaboration

A measurement of vector boson scattering and constraints on anomalous quartic gauge couplings from events with two Z bosons and two jets are presented. The analysis is based on a data sample of proton-proton collisions at root s = 13 TeV collected with the CMS detector and corresponding to an integrated luminosity of 35.9 fb(-1). The search is performed in the fully leptonic final state ZZ -> lll'l', where l, l' = e or mu. The electroweak production of two Z bosons in association with two jets is measured with an observed (expected) significance of 2.7 (1.6) standard deviations. A fiducial cross section for the electroweak production is measured to be sigma(EW)(PP -> ZZjj -> lll'l'jj') =0.40(-0.16)(+0.21)(stat) (+0.13)(-0.009)(syst) fb, which is consistent with the standard model prediction. Limits on anomalous quartic gauge couplings are determined in terms of the effective field theory operators T0, T1, T2, T8, and T9. This is the first measurement of vector boson scattering in the ZZ channel at the LHC.

PHYSICS LETTERS B 774, 682-705, 2017. DOI: 10.1016/j.physletb.2017.10.020

[P354-2017] "Measuring (KSK +/-)-K-0 interactions using Pb--Pb collisions at root S-NN=2.76 TeV"

Acharya, S.; Adamova, D.; Adolfsson, J.; **Albuquerque, D. S. D.*; Chinellato, D. D.*; De Souza, R. D.*; Takahashi, J.***; et al.
ALICE Collaboration

We present the first ever measurements of femtoscopic correlations between the K-S(0) and K-+/- particles. The analysis was performed on the data from Pb-Pb collisions at root S-NN = 2.76 TeV measured by the ALICE experiment. The observed femtoscopic correlations are consistent with final--state interactions proceeding via the a(0)(980) resonance. The extracted kaon source radius and correlation strength parameters for (KSK-)-K-0 are found to be equal within the experimental uncertainties to those for (KSK+)-K-0. Comparing the results of the present study with those from published identical-kaon femtoscopic studies by ALICE, mass and coupling parameters for the a(0) resonance are tested. Our results are also compatible with the interpretation of the a(0) having a tetraquark structure instead of that of a diquark.

PHYSICS LETTERS B 774, 64-77, 2017. DOI: 10.1016/j.physletb.2017.09.009

[P355-2017] "Microcanonical Szilard engines beyond the quasistatic regime"

Acconcia, T. V.*; Bonanca, M. V. S.*

We discuss the possibility of extracting energy from a single thermal bath using microcanonical Szilard engines operating in finite time. This extends previous works on the topic which are restricted to the quasistatic regime. The feedback protocol is implemented based on linear response predictions of the excess work. It is claimed that the underlying mechanism leading to energy extraction does not violate Liouville's theorem and preserves ergodicity throughout the cycle. We illustrate our results with several examples including an exactly solvable model.

PHYSICAL REVIEW E 96[6], 062117, 2017. DOI: 10.1103/PhysRevE.96.062117

[P356-2017] "Multifunctional Hybrids Based on 2D Fluorinated Graphene Oxide and Superparamagnetic Iron Oxide Nanoparticles"

Radhakrishnan, S.; Sudeep, P. M.; Park, J. H.; **Woellner, C. F.***; Maladonado, K.; **Galvao, D. S.***; Kaipparettu, B. A.; Tiwary, C. S.; Ajayan, P. M.

Carbon-based nanomaterials have garnered a lot of attention in the research of yesteryear. Here this study reports a composite based on fluorinated graphene oxide-a multifunctional subsidiary of graphene; and iron oxide nano-particles as a contrast agent for magnetic resonance imaging (MRI). Extensive structural and functional characterization is carried out to understand composite behavior toward biotoxicity and its performance as a contrast agent. The electron withdrawing fluorine group decreases the charge transfer to iron oxide increasing the magnetic saturation of the composite thus enhancing the contrast. The interaction of paramagnetic and superparamagnetic systems yields a superior contrast agent for MRI and fluorescent imaging.

PARTICLE & PARTICLE SYSTEMS CHARACTERIZATION 34[11], 1700245, 2017. DOI: 10.1002/ppsc.201700245

[P357-2017] "Numerical insight into the Dual Radiation Action Theory"

Tello, J. J.*; Incerti, S.; Francis, Z.; Tran, H.; **Bernal, M. A.***

This work studies the first and second order mechanisms for the induction of lethal lesions in DNA after irradiation with protons and alpha-particles. The purpose is to numerically study the mechanisms behind the Dual Radiation Action Theory (DRAT) for these heavy particles. A genetic material geometrical model with atomic resolution is used. It accounts for the explicit position of 5.47x10(9) base pairs, organized up to the chromatin level. The GEANT4-DNA Monte Carlo code was employed to simulate the interaction of these ions with the genetic material model. The number of lethal lesions induced by one-and two--track mechanisms was determined as a function of dose. Values of the alpha/beta ratio were estimated as well as corresponding relative biological effectiveness (RBE). The number of lethal lesions produced by one-track and two-track mechanisms depends on the dose and squared dose, respectively, as predicted by the DRAT. RBE values consistent with experimental results were found, at least for LET below similar to 100 keV/mu m. Double strand break spatial distributions are qualitatively analyzed. According to this work, the alpha parameter determined from cellular surviving curves depends on both the physical alpha and beta parameters introduced here, and on the specific energy deposited by a single track into the region of interest. We found an increment of the beta parameter with LET, yet at a slower rate than alpha so that the alpha/beta ratio increases with LET. In addition, we observed and explained the saturation of the alpha parameter as the dose increases above similar to 6 Gy.

PHYSICA MEDICA-EUROPEAN JOURNAL OF MEDICAL PHYSICS 43, 120-126, 2017. DOI: 10.1016/j.ejmp.2017.10.022

[P358-2017] "Observation of Top Quark Production in Proton-Nucleus Collisions"

Sirunyan, A. M.; Turnasyan, A.; Adam, W.; **Chinellato, J. A.*; Tonelli Manganote, E. J.***; et al.
CMS Collaboration

The first observation of top quark production in proton-nucleus collisions is reported using proton-lead data collected by the CMS experiment at the CERN LHC at a nucleon-nucleon center-of-mass energy of root(S)(NN) = 8.16 TeV. The measurement is performed using events with exactly one isolated electron or muon candidate and at least four jets. The data sample corresponds to an integrated luminosity of 174 nb(-1). The significance of the tt signal against the background--only hypothesis is above 5 standard deviations. The measured cross section is sigma(tt) = 45 +/- 8 nb, consistent with predictions from perturbative quantum chromodynamics.

PHYSICAL REVIEW LETTERS 119[24], 242001, 2017. DOI: 10.1103/PhysRevLett.119.242001

[P359-2017] "On the influence of thermal hysteresis on the performance of thermomagnetic motors"

Bessa, C. V. X.; Ferreira, L. D. R.; Horikawa, O.; **Monteiro, J. C. B.*; Gandra, F. G.***; Gama, S.

Although thermal hysteresis might be a problem in the magnetocaloric refrigeration, the same is not necessarily true for thermomagnetic motor applications. This work presents a comparison of the magnetocaloric properties of materials with first order magnetic transition (having large or narrow thermal hysteresis) to those with second order magnetic transition, assessing the application of these materials in thermomagnetic motors through a thermodynamic approach. Results show that the larger the thermal hysteresis, the higher the specific work produced in a thermal cycle. This allows operation at higher temperature differences with high efficiency relative to Carnot efficiency, when compared with systems using narrow hysteresis and second order transition materials.

JOURNAL OF APPLIED PHYSICS 122[24], 244502, 2017. DOI: 10.1063/1.5010356

[P360-2017] "Optical image cloning based on electromagnetic induced absorption"

Apolinario, U. F.*; Manzoor, S.*; Araujo, L. E. E.*

We investigate, both theoretically and experimentally, optical image cloning via electromagnetic induced absorption (EIA). We demonstrate the transfer of small 2D real images imprinted onto a strong coupling beam to a weak probe beam in a Rb vapor cell. We show through EIA that the coupling beam's image is cloned beyond the usual diffraction, with a potential improvement in spatial resolution of the cloned image by a factor of three in comparison to that of the original coupling beam.

Optical cloning through EIA is based on position selective nonlinear absorption, and it does not rely on spatial modulation of the refractive index.

OPTICS LETTERS 42[23], 4966-4969, 2017. DOI: 10.1364/OL.42.004966

[P361-2017] "Principal-component analysis of two-particle azimuthal correlations in PbPb and pPb collisions at CMS"

Sirunyan, A. M.; Turnasyan, A.; Adam, W.; **Chinellato, J. A.*; Tonelli Manganote, E. J.***; et al.
CMS Collaboration

For the first time a principle-component analysis is used to separate out different orthogonal modes of the two-particle correlation matrix from heavy ion collisions. The analysis uses data from root s(NN) = 2.76 TeV PbPb and root s(NN) = 5.02 TeV pPb collisions collected by the CMS experiment at the CERN Large Hadron Collider. Two-particle azimuthal correlations have been extensively used to study hydrodynamic flow in heavy ion collisions. Recently it was shown that the expected factorization of two-particle results into a product of the constituent single-particle anisotropies is broken. The new information provided by these modes may shed light on the breakdown of flow factorization in heavy ion collisions. The first two modes ("leading" and "subleading") of two-particle correlations are presented for elliptical and triangular anisotropies in PbPb and pPb collisions as a function of p(T) over a wide range of event activity. The leading mode is found to be essentially equivalent to the anisotropy harmonic previously extracted from two--particle correlation methods. The subleading mode represents a new experimental observable and is shown to account for a large fraction of the factorization breaking recently observed at high transverse momentum. The principle-component analysis technique was also applied to multiplicity fluctuations. These also show a subleading mode. The connection of these new results to previous studies of factorization is discussed.

PHYSICAL REVIEW C 96[6], 064902, 2017. DOI: 10.1103/PhysRevC.96.064902

[P362-2017] "Radioactive source calibration test of the CMS Hadron Endcap Calorimeter test wedge with Phase I upgrade electronics"

Chatrchyan, S.; Sirunyan, A. M.; Turnasyan, A.; **Chinellato, J. A.*; Tonelli Manganote, E. J.***; et al.
CMS HCAL Collaboration

The Phase I upgrade of the CMS Hadron Endcap Calorimeters consists of new photodetectors (Silicon Photomultipliers in place of Hybrid Photo-Diodes) and front-end electronics. The upgrade will eliminate the noise and the calibration drift of the Hybrid Photo-Diodes and enable the mitigation of the radiation damage of the scintillators and the wavelength shifting fibers with a larger spectral acceptance of the Silicon Photomultipliers. The upgrade also includes increased longitudinal segmentation of the calorimeter readout, which allows pile-up mitigation and recalibration due to depth--dependent radiation damage. As a realistic operational test, the responses of the Hadron Endcap Calorimeter wedges were calibrated with a Co-60 radioactive source with upgrade electronics. The test successfully established the procedure for future source calibrations of the Hadron Endcap Calorimeters. Here we describe the instrumentation details and the operational experiences related to the sourcing test.

JOURNAL OF INSTRUMENTATION 12, P12034, 2017. DOI: 10.1088/1748-0221/12/12/P12034

[P363-2017] "Scattering cross section and stability of global monopoles"

Pitelli, J. P. M.; **Barroso, V. S.***; Richartz, M.

We study the scattering of scalar waves propagating on the global monopole background. Since the scalar wave operator in this topological defect is not essentially self-adjoint, its solutions are not uniquely determined until a boundary condition at the origin is specified. As we show, this boundary condition manifests itself in the differential cross section and can be inferred by measuring the amplitude of the backscattered wave. We further demonstrate that whether or not the spacetime is stable under scalar perturbations also depends on the chosen boundary condition. In particular, we identify a class of such boundary conditions that significantly affects the differential cross section without introducing an instability.

PHYSICAL REVIEW D 96[10], 105021, 2017. DOI: 10.1103/PhysRevD.96.105021

[P364-2017] "Search for a heavy composite Majorana neutrino in the final state with two leptons and two quarks at root s=13 TeV"

Sirunyan, A. M.; Turnasyan, A.; Adam, W.; **Chinellato, J. A.*; Tonelli Manganote, E. J.***; et al.
CMS Collaboration

A search for physics beyond the standard model in the final state with two same-flavour leptons (electrons or muons) and two quarks produced in proton-proton collisions at root s = 13 TeVis presented. The data were recorded by the CMS experiment at the CERN LHC and correspond to an integrated luminosity of 2.3 fb(-1). The observed data are in good agreement with the standard model background prediction. The results of the measurement are interpreted in the framework of a recently proposed model in which a heavy Majorana neutrino, N-l, stems from a composite-fermion scenario. Exclusion limits are set for the first time on the mass of the heavy composite Majorana neutrino, m(Nl), and the compositeness scale Lambda. For the case m(Nl) = Lambda, the existence of N-e (N-mu) is excluded for masses up to 4.60 (4.70) TeV at 95% confidence level.

PHYSICS LETTERS B 775, 315-337, 2017. DOI: 10.1016/j.physletb.2017.11.001

[P365-2017] "Search for anomalous couplings in boosted WW/WZ -> l upsilon q(q)over-bar production in proton-proton collisions at root s=8TeV"

Sirunyan, A. M., Tumasyan, A., Adam, W.; **Chinellato, J. A.*; Tonelli Manganote, E. J.***; et al.
CMS Collaboration

This Letter presents a search for new physics manifested as anomalous triple gauge boson couplings in WW and WZ diboson production in proton-proton collisions. The search is performed using events containing a W boson that decays leptonically and a W or Zboson whose decay products are merged into a single reconstructed jet. The data, collected at root s= 8TeVwith the CMS detector at the LHC, correspond to an integrated luminosity of 19 fb(-1). No evidence for anomalous triple gauge couplings is found and the following 95% confidence level limits are set on their values: lambda([-0.011, 0.011]), Delta(kappa gamma)([-0.044, 0.063]), and Delta g(1)(Z)([-0.0087, 0.024]). These limits are also translated into their effective field theory equivalents: c(WWW)/Lambda(2)([- 2.7, 2.7] TeV-2), c(B)/Lambda(2)([-14, 17] TeV-2), and cW/Lambda(2)([- 2.0, 5.7] TeV-2).

PHYSICS LETTERS B 772, 21-42, 2017. DOI: 10.1016/j.physletb.2017.06.009

[P366-2017] "Search for black holes and other new phenomena in high-multiplicity final states in proton-proton collisions at root s=13 TeV"

Sirunyan, A. M.; Turnasyan, A.; Adam, W.; **Chinellato, J. A.*; Tonelli Manganote, E. J.***; et al.
CMS Collaboration

A search for new physics in energetic, high-multiplicity final states has been performed using proton-proton collision data collected with the CMS detector at a center-of-mass energy of 13 TeV and corresponding to an integrated luminosity of 2.3 fb(-1). The standard model background, dominated by multijet production, is determined exclusively from control regions in data. No statistically significant excess of events is observed. Model--independent limits on the product of the cross section and the acceptance of a new physics signal in these final states are set and further interpreted in terms of limits on the production of black holes. Semiclassical black holes and string balls with masses as high as 9.5 TeV, and quantum black holes with masses as high as 9.0 TeV are excluded by this search in the context of models with extra dimensions, thus significantly extending limits set at a center-of-mass energy of 8 TeV with the LHC Run 1 data.

PHYSICS LETTERS B 774, 279-307, 2017. DOI: 10.1016/j.physletb.2017.09.053

[P367-2017] "Search for dark matter produced in association with heavy-flavor quark pairs in proton-proton collisions at root s=13 TeV"

Sirunyan, A. M.; Turnasyan, A.; Adam, W.; **Chinellato, J. A.*; Tonelli Manganote, E. J.***; et al.
CMS Collaboration

A search is presented for an excess of events with heavy-flavor quark pairs (t (t) over bar and b (b) over bar) and a large imbalance in transverse momentum in data from proton-proton collisions at a center-of-mass energy of 13 TeV. The data correspond to an integrated luminosity of 2.2 fb(-1) collected with the CMS detector at the CERN LHC. No deviations are observed with respect to standard model predictions. The results are used in the first interpretation of dark matter production in t (t) over bar and b (b) over bar final states in a simplified model. This analysis is also the first to perform a statistical combination of searches for dark matter produced with different heavy-flavor final states. The combination provides exclusions that are stronger than those achieved with individual heavy-flavor final states.

EUROPEAN PHYSICAL JOURNAL C 77[12], 845, 2017. DOI: 10.1140/epjc/s10052-017-5317-4

[P368-2017] "Search for electroweak production of charginos and neutralinos in WH events in proton-proton collisions at root s=13 TeV"

Sirunyan, A. M.; Turnasyan, A.; Adam, W.; **Chinellato, J. A.*; Tonelli Manganote, E. J.*;** et al.
CMS Collaboration

Results are reported from a search for physics beyond the standard model in proton-proton collision events with a charged lepton (electron or muon), two jets identi fi ed as originating from a bottom quark decay, and signi fi cant imbalance in the transverse momentum. The search was performed using a data sample corresponding to 35.9 fb(-1), collected by the CMS experiment in 2016 at root s = 13 TeV. Events with this signature can arise, for example, from the electroweak production of gauginos, which are predicted in models based on supersymmetry. The event yields observed in data are consistent with the estimated standard model backgrounds. Limits are obtained on the cross sections for chargino-neutralino ((chi) over tilde (+/-)(1) (chi) over tilde (0)(2)) production in a simplified model of supersymmetry with the decays (chi) over tilde (+/-)(1) -> W-(chi) over tilde1(+/-)0 and (chi) over tilde (0)(2) -> H-(chi) over tilde1(0). Values of m((chi) over tilde1 +/-) between 220 and 490 GeV are excluded at 95% confidence level by this search when the (chi) over tilde (0)(1) is massless, and values of m((chi) over tilde 10) are excluded up to 110 GeV for m((chi) over tilde1 +/-) approximate to 450 GeV.

JOURNAL OF HIGH ENERGY PHYSICS 11, 029, 2017. DOI: 10.1007/JHEP11(2017)029

[P369-2017] "Search for Evidence of the Type-III Seesaw Mechanism in Multilepton Final States in Proton-Proton Collisions at root s=13 TeV"

Sirunyan, A. M.; Turnasyan, A.; Adam, W.; **Chinellato, J. A.*; Tonelli Manganote, E. J.***; et al.
CMS Collaboration

A search for a signal consistent with the type-III seesaw mechanism in events with three or more electrons or muons is presented. The data sample consists of proton-proton collisions at root s = 13 TeV collected by the CMS experiment at the LHC in 2016 and corresponds to an integrated luminosity of 35.9 fb(-1). Selection criteria based on the number of leptons and the invariant mass of oppositely charged lepton pairs are used to distinguish the signal from the standard model background. The observations are consistent with the expectations from standard model processes. The results are used to place limits on the production of heavy fermions of the type-III seesaw model as a function of the branching ratio to each lepton flavor. In the scenario of equal branching fractions to each lepton flavor, heavy fermions with masses below 840 GeV are excluded. This is the most sensitive probe to date of the type-III seesaw mechanism.

PHYSICAL REVIEW LETTERS 119[22], 221802, 2017. DOI: 10.1103/PhysRevLett.119.221802

[P370-2017] "Search for High-energy Neutrinos from Binary Neutron Star Merger GW170817 with ANTARES, IceCube, and the Pierre Auger Observatory"

Albert, A.; Andre, M.; Anghinolfi, M.; **Chinellato, J. A*.; Daniel, B.*; Diaz Castro, M. L.*; Dobrigkeit, C.*; Fauth, A. C.*; Muller, M. A.*; Pereira, L. A. S.***; et al.
ANTARES Collaboration; IceCube Collaboration; Pierre Auger Collaboration; LIGO Sci Collaboration & Virgo

The Advanced LIGO and Advanced Virgo observatories recently discovered gravitational waves from a binary neutron star inspiral. A short gamma-ray burst (GRB) that followed the merger of this binary was also recorded by the Fermi Gamma-ray Burst Monitor (Fermi-GBM), and the Anti-Coincidence Shield for the Spectrometer for the International Gamma-Ray Astrophysics Laboratory (INTEGRAL), indicating particle acceleration by the source. The precise location of the event was determined by optical detections of emission following the merger. We searched for high-energy neutrinos from the merger in the GeV-EeV energy range using the ANTARES, IceCube, and Pierre Auger Observatories. No neutrinos directionally coincident with the source were detected within +/- 500 s around the merger time. Additionally, no MeV neutrino burst signal was detected coincident with the merger. We further carried out an extended search in the direction of the source for high-energy neutrinos within the 14 day period following the merger, but found no evidence of emission. We used these results to probe dissipation mechanisms in relativistic outflows driven by the binary neutron star merger. The non-detection is consistent with model predictions of short GRBs observed at a large off-axis angle.

ASTROPHYSICAL JOURNAL LETTERS 850[2], L35, 2017. DOI: 10.3847/2041-8213/aa9aed

[P371-2017] "Search for pair production of vector-like T and B quarks in single-lepton final states using boosted jet substructure in proton-proton collisions at root s=13 TeV"

Sirunyan, A. M.; Turnasyan, A.; Adam, W.; **Chinellato, J. A.*; Tonelli Manganote, E. J.***; et al.
CMS Collaboration

A search for pair production of massive vector-like T and B quarks in proton-proton collisions at root s = 13 TeV is presented. The data set was collected in 2015 by the CMS experiment at the LHC and corresponds to an integrated luminosity of up to 2.6 fb(-1). The T and B quarks are assumed to decay through three possible channels into a heavy boson (either a W, Z or Higgs boson) and a third generation quark. This search is performed in final states with one charged lepton and several jets, exploiting techniques to identify W or Higgs bosons decaying hadronically with large transverse momenta. No excess over the predicted standard model background is observed. Upper limits at 95% confidence level on the T quark pair production cross section are set that exclude T quark masses below 860 GeV in the singlet, and below 830 GeV in the doublet branching fraction scenario. For other branching fraction combinations with B (T -> tH) + B(T -> bW) >= 0.4, lower limits on the T quark range from 790 to 940 GeV. Limits are also set on pair production of singlet vector-like B quarks, which can be excluded up to a mass of 730 GeV. The techniques showcased here for understanding highly-boosted final states are important as the sensitivity to new particles is extended to higher masses.

JOURNAL OF HIGH ENERGY PHYSICS 11, 085, 2017. DOI: 10.1007/JHEP11(2017)085

[P372-2017] "Search for supersymmetry in events with at least one photon, missing transverse momentum, and large transverse event activity in proton-proton collisions at root s=13TeV"

Sirunyan, A. M.; Tumasyan, A.; Adam, W.; **Chinellato, J. A.*; Tonelli Manganote, E. J.***; et al.
CMS collaboration

A search for physics beyond the standard model in final states with at least one photon, large transverse momentum imbalance, and large total transverse event activity is presented. Such topologies can be produced in gauge-mediated supersymmetry models in which pair-produced gluinos or squarks decay to photons and gravitinos via shortlived neutralinos. The data sample corresponds to an integrated luminosity of 35.9 fb(-1) of proton--proton collisions at root s = 13TeV recorded by the CMS experiment at the LHC in 2016. No significant excess of events above the expected standard model background is observed. The data are interpreted in simplified models of gluino and squark pair production, in which gluinos or squarks decay via neutralinos to photons. Gluino masses of up to 1.50-2.00TeV and squark masses up to 1.30-1.65TeV are excluded at 95% confidence level, depending on the neutralino mass and branching fraction.

JOURNAL OF HIGH ENERGY PHYSICS [12], 142, 2017. DOI: 10.1007/JHEP12(2017)142

[P373-2017] "Search for Supersymmetry in pp Collisions at root s=13 TeV in the Single-Lepton Final State Using the Sum of Masses of Large-Radius Jets"

Sirunyan, A. M.; Turnasyan, A.; Adam, W.; **Chinellato, J.*; Tonelli Manganote, E. J.***; et al.
CMS Collaboration

Results are reported from a search for supersymmetric particles in proton-proton collisions in the final state with a single lepton, multiple jets, including at least one b-tagged jet, and large missing transverse momentum. The search uses a sample of proton-proton collision data at root s = 13 TeV recorded by the CMS experiment at the LHC, corresponding to an integrated luminosity of 35.9 fb(-1). The observed event yields in the signal regions are consistent with those expected from standard model backgrounds. The results are interpreted in the context of simplified models of supersymmetry involving gluino pair production, with gluino decay into either on- or off-mass--shell top squarks. Assuming that the top squarks decay into a top quark plus a stable, weakly interacting neutralino, scenarios with gluino masses up to about 1.9 TeV are excluded at 95% confidence level for neutralino masses up to about 1 TeV.

PHYSICAL REVIEW LETTERS 119[15], 151802, 2017. DOI: 10.1103/PhysRevLett.119.151802

[P374-2017] "Side-lobe level reduction in bio-inspired optical phased-array antennas"

Pita, J. L.; **Aldaya, I.*; Santana, O. J. S.*; De Araujo, L. E. E.*; Dainese, P.***; Gabrielli, L. H.

Phased arrays are expected to play a critical role in visible and infrared wireless systems. Their improved performance compared to single element antennas finds uses in communications, imaging, and sensing. However, fabrication of photonic antennas and their feeding network require long element separation, leading to the appearance of secondary radiation lobes and, consequently, crosstalk and interference. In this work, we experimentally show that by arranging the elements according to the Fermat's spiral, the side lobe level (SLL) can be reduced. This reduction is proved in a CMOS-compatible 8-element array, revealing a SLL decrement of 0.9 dB. Arrays with larger numbers of elements and inter-element spacing are demonstrated through a spatial light modulator (SLM) and an SLL drop of 6.9 dB is measured for a 64-element array. The reduced SLL, consequently, makes the proposed approach a promising candidate for applications in which antenna gain, power loss, or information security are key requirements.

OPTICS EXPRESS 25[24], 30105-30114, 2017. DOI: 10.1364/OE.25.030105

[P375-2017] "Silicon Nanomembranes with Hybrid Crystal Orientations and Strain States"

Scott, S. A.; **Deneke, C.***; Paskiewicz, D. M.; Ryu, H. J.; Malachias, A.; Baunack, S.; Schmidt, O. G.; Savage, D. E.; Eriksson, M. A.; Lagally, M. G.

Methods to integrate different crystal orientations, strain states, and compositions of semiconductors in planar and preferably flexible configurations may enable nontraditional sensing-, stimulating-, or communication-device applications. We combine crystalline-silicon nanomembranes, patterning, membrane transfer, and epitaxial growth to demonstrate planar arrays of different orientations and strain states of Si in a single membrane, which is then readily transferable to other substrates, including flexible supports. As examples, regions of Si(001) and Si(110) or strained Si(110) are combined to form a multicomponent, single substrate with high-quality narrow interfaces. We perform extensive structural characterization of all interfaces and measure charge-carrier mobilities in different regions of a 2D quilt. The method is readily extendable to include varying compositions or different classes of materials.

ACS APPLIED MATERIALS & INTERFACES 9[48], 2017. 42372-42382 DOI: 10.1021/acsami.7b14291

[P376-2017] "Size effects of the magnetic anisotropy of fcc cobalt nanoparticles embedded in copper"

Hillenkamp, M.*; Oyarzun, S.; Troc, N.; Ramade, J.; Tamion, A.; Tournus, F.; Dupuis, V.; **Rodrigues, V.***

Cobalt nanoparticles embedded in copper matrices show strong size effects in the magnetic anisotropy with a non--monotonous dependence on the particle diameter. In this article we discuss quantitative values of the magnetic anisotropy in the frame of two models: in small clusters the surface anisotropy contribution dominates whereas larger particles (>3 nm diameter) have an elliptic shape leading to increased shape anisotropy. The crystalline structure of the particles is shown to be face-centered cubic, justifying that the magneto-crystalline anisotropy can be neglected.

EUROPEAN PHYSICAL JOURNAL D 71[12], 330, 2017. DOI: 10.1140/epjd/e2017-80299-x

[P377-2017] "Stiffness signatures along early stages of Xylella fastidiosa biofilm formation"

Monteiro, M. P.*; Clerici, J. H.*; Sahoo, P. K.*; Cesar, C. L.*; de Souza, A. A.; **Cotta, M. A.***

The pathogenicity of Xylella fastidiosa is associated with its systematic colonization of the plant xylem, forming bacterial biofilms. Mechanisms of bacterial transport among different xylem vessels, however, are not completely understood yet, but are strongly influenced by the presence of extracellular polymeric substances (EPS), which surrounds the assembly of cells forming the biofilm. In this work, we show quantitative measurements on the elastic properties of the system composed by EPS and bacterial cell. In order to investigate the mechanical properties of this system, force spectroscopy and confocal Raman measurements were carried out during Xylella fastidiosa subsp. pauca initial stages of adhesion and cluster formation. We show that stiffness progressively decreases with increasing culture growth time, from two to five days. For early adhesion samples, stiffness values are quite different at the bacterial polar and body regions. Lower stiffness values at the cell pole suggest a flexible mechanical, response at this region, associated with first cell adhesion to a surface. These results correlate very well with our observations of cell motion within microchannels, under conditions simulating xylem flow. Both the oscillatory movement of vertically attached single cells, as well as the transport of cell clusters within the biofilm matrix can be explained by the presence of softer materials at the cell pole and EPS matrix. Our results may thus add to a more detailed understanding of mechanisms used by cells to migrate among vessels in plant xylem.

COLLOIDS AND SURFACES B-BIOINTERFACES 159, 174-182, 2017. DOI: 10.1016/j.colsurfb.2017.07.075

[P378-2017] "Synthesis process, size and composition effects of spherical Fe3O4 and FeO@Fe3O4 core/shell nanoparticles"

Tancredi, P.; Rivas R., Patricia C.; **Moscoso-Londono, O.***; Wolff, U.; Neu, V.; Damm, C.; Rellinghaus, B.; **Knobel, M.***; Socolovsky, L. M.

In this work, we investigate the size, composition and magnetic behavior of a series of iron oxide nanoparticles prepared by means of high temperature decomposition of an iron oleate precursor. Different synthesis conditions, such as gas atmosphere, precursor ratio and heating rate were tested to obtain a direct correlation between the final sample structure and the varied parameter. The synthesis products were characterized by X-ray diffraction, transmission electron microscopy and small-angle X-ray scattering, respectively. We studied six samples with rather narrow size distribution and mean diameters from 8 nm to 16 nm. The particles with diameter below 11 nm were found to be spinel-type, monocrystalline, and their magnetic response can be ascribed to a single domain framework. On the other hand, two-phase core-shell FeO@Fe3O4 of mean sizes of 15 nm and 16 nm were obtained by increasing the amount of oleic acid and the heating rate. The magnetic behavior of these samples exhibits interesting interface features, related to the exchange coupling phenomenon between the FeO and Fe3O4. We discuss how the different synthesis conditions may lead to the presence of this FeO phase, and how the core-shell configuration and other structural features affect the macroscopic magnetic behavior.

NEW JOURNAL OF CHEMISTRY 41[24], 15033-15041, 2017. DOI: 10.1039/c7nj02558k

[P379-2017] "The Deep Underground Neutrino Experiment: The precision era of neutrino physics"

Kemp, E.*;
DUNE Collaboration

The last decade was remarkable for neutrino physics. In particular, the phenomenon of neutrino flavor oscillations has been firmly established by a series of independent measurements. All parameters of the neutrino mixing are now known, and we have the elements to plan a judicious exploration of new scenarios that are opened by these recent advances. With precise measurements, we can test the three-neutrino paradigm, neutrino mass hierarchy, and charge conjugation parity (CP) asymmetry in the lepton sector. The future long-baseline experiments are considered to be a fundamental tool to deepen our knowledge of electroweak interactions. The Deep Underground Neutrino Experiment (DUNE) will detect a broadband neutrino beam from Fermilab in an underground massive liquid argon time-projection chamber at an L/E of about 10(3) km GeV-1 to reach good sensitivity for CP-phase measurements and the determination of the mass hierarchy. The dimensions and the depth of the far detector also create an excellent opportunity to look for rare signals like proton decay to study violation of the baryonic number, as well as supernova neutrino bursts, broadening the scope of the experiment to astrophysics and associated impacts in cosmology. In this paper, we discuss the physics motivations and the main experimental features of the DUNE project required to reach its scientific goals.

ASTRONOMISCHE NACHRICHTEN 338[9-10], [SI], 993-999, 2017. DOI: 10.1002/asna.201713417

[P380-2017] "The electronics, trigger and data acquisition system for the liquid argon time projection chamber of the DarkSide-50 search for dark matter"

Agnes, P.; Albuquerque, I. F. M.; Alexander, T.; **Segreto, E.***; et al.
DarkSide Collaboration

The DarkSide-50 experiment at the Laboratori Nazionali del Gran Sasso is a search for dark matter using a dual phase time projection chamber with 50 kg of low radioactivity argon as target. Light signals from interactions in the argon are detected by a system of 38 photo-multiplier tubes (PMTs), 19 above and 19 below the TPC volume inside the argon cryostat. We describe the electronics which processes the signals from the photo-multipliers, the trigger system which identifies events of interest, and the data-acquisition system which records the data for further analysis. The electronics include resistive voltage dividers on the PMTs, custom pre-amplifiers mounted directly on the PMT voltage dividers in the liquid argon, and custom amplifier/discriminators (at room temperature). After amplification,

the PMT signals are digitized in CAEN waveform digitizers, and CAEN logic modules are used to construct the trigger; the data acquisition system for the TPC is based on the Fermilab artdaq software. The system has been in operation since early 2014.

JOURNAL OF INSTRUMENTATION 12, P12011, 2017. DOI: 10.1088/1748-0221/12/12/P12011

[P381-2017] "Thermoelectricity Enhanced Electrocatalysis"

Sharifi, T.; Zhang, X.; Costin, G.; Yazdi, S.; **Woellner, C. F.***; Liu, Y.; Tiwary, C. S.; Ajayan, P.

We show that thermoelectric materials can function as electrocatalysts and use thermoelectric voltage generated to initiate and boost electrocatalytic reactions. The electrocatalytic activity is promoted by the use of nano-structured thermoelectric materials in a hydrogen evolution reaction (HER) by the thermoelectricity generated from induced temperature gradients. This phenomenon is demonstrated using two-dimensional layered thermoelectric materials Sb2Te3 and Bi0.5Sb1.5Te3 where a current density approaching similar to 50 mA/cm(2) is produced at zero potential for Bi0.5Sb1.5Te3 in the presence of a temperature gradient of 90 degrees C. In addition, the turnover frequency reaches to 2.7 s(-1) at 100 mV under this condition which was zero in the absence of temperature gradient. This result adds a new dimension to the properties of thermoelectric materials which has not been explored before and can be applied in the field of electrocatalysis and energy generation.

NANO LETTERS 17[12], 7908-7913, 2017. DOI: 10.1021/acs.nanolett.7b04244

[P382-2017] "Time-Resolved X-Ray Powder Diffraction Study of Photoinduced Phase Transitions in Ti3O5 Nanoparticles"

Tasca, K. R.*; Esposito, V.; Lantz, G.; Beaud, P.; Kubli, M.; Savoini, M.; **Giles, C.***; Johnson, S. L.

Nanoparticles of Ti3O5 have been reported to show a permanent photoinduced phase transition at room temperature. This suggests that light-induced phase transformations of Ti3O5 nanoparticles may be promising for technological applications. Here, we report a photoinduced semiconductor--to-metal phase transition from beta-Ti3O5 to lambda-Ti3O5 nanoparticles at room temperature observed directly by time--resolved X-ray powder diffraction in a pump-probe setup. The results show a partial structural change, limited by differences between pumped and probed volumes, which persists a few microseconds after excitation. The first step in the relaxation back to the ground state can be described by a single exponential decay with time constant within microsecond timescales. Analysis of the change in lattice constants enables us to estimate an average temperature increase across the phase transition, consistent with a thermally driven process.

CHEMPHYSCHEM 18[10], 1385-1392, 2017. DOI: 10.1002/cphc.201601337

[P383-2017] "Topical use and systemic action of green and roasted coffee oils and ground oils in a cutaneous incision model in rats (Rattus norvegicus albinus)"

Lania, B. G.; Morari, J.; de Souza, A. L.; da Silva, M. N.; de Almeida, A. R.; Veira-Damiani, G.; Alegre, S. M.; **Cesar, C. L.***; Velloso, L. A.; Cintra, M. L.; Mala, N. B.; Neves Ferreira Velho, P. E.

Introduction: Wounds are a common health problem. Coffee is widely consumed and its oil contains essential fatty acids. We evaluated the local (skin) and systemic effects associated with the topical use of coffee oils in rats. Methods: Punch skin wounds (6 mm) incisions were generated on the backs of 75 rats. Saline (SS), mineral oil (MO), green coffee oil (GCO), roasted coffee oil (RCO), green coffee ground oil (GCGO) or roasted coffee ground oil (RCGO) were topically applied to the wounds. Healing was evaluated by visual and histological/morphometric optical microscopy examination; second harmonics generation (SHG) microscopy, wound tissue q-PCR (values in fold--change) and blood serum (ELISA, values in pg/mL). Results: RCO treated animals presented faster wound healing (0.986 vs. 0.422), higher mRNA expression of IGF-1 (2.78 vs. 1.00, p = 0.01), IL-6 (10.72 vs. 1.00, p = 0.001) and IL-23 (4.10 vs. 1.2, p = 0.05) in early stages of wound healing; higher IL-12 (3.32 vs. 1.00, p = 0.05) in the later stages; and lower serum levels of IFN-gamma (11.97 vs. 196.45, p = 0.01). GCO treatment led to higher mRNA expression of IL-6 (day 2: 7.94 vs. 1.00, p = 0.001 and day 4: 6.90 vs. 1.00, p = 0.01) and IL-23 (7.93 vs. 1.20, p = 0.001) in the early stages. The RCO treatment also produced higher serum IFN-alpha levels throughout the experiment (day 2: 52.53 vs. 21.20; day 4: 46.98 vs. 21.56; day 10: 83.61 vs. 25.69, p = 0.05) and lower levels of IL-4 (day 4: 0.9 vs. 13.36, p = 0.01), adiponectin (day 10: 8,367.47 vs. 16,526.38, p = 0.001) and IFN-gamma (day 4: 43.03 vs. 196.45, p = 0.05). The SHG analysis showed a higher collagen density in the RCO and GCO treatments (p = 0.05). Conclusion: Topical treatment with coffee oils led to systemic actions and faster wound healing in rats. Further studies should be performed are necessary to assess the safety of topical vegetal oil use for skin lesions.

PLOS ONE 12[12], e0188779, 2017. DOI: 10.1371/journal.pone.0188779

[P384-2017] "Transient anion spectra of the potential radiosensitizers 5-cyanateuracil and 5-thiocyanateuracil"

Cornetta, L. M.; **Kossoski, F.***; Varella, M. T. do N.

We report on the low energy anion spectra of 5-cyanateuracil (5-OCNU) and 5-thiocyanateouracil (5-SCNU), which have been the suggested potential radiosensitizers for use in cancer therapy [L. Chomicz et al., J. Phys. Chem. Lett. 4, 2853-2857 (2013)]. Employing bound state and scattering calculations, we obtained, for both molecules, a dipole bound state, a pi* valence bound state, and four pi* resonances, besides a sigma*(SCN) resonance for 5-SCNU. The cyanate and thiocyanate sub-stituents give rise to additional long-lived pi* resonances, compared to 5-halouracil radiosensitizers. From the reaction thresholds and the expected vibronic couplings among the anion states, efficient production of SCN and CN anions and radical fragments should be observed in dissociative electron attachment measurements for 5-SCNU. The corresponding dissociation processes in 5-OCNU are expected to be less effective in view of the lack of a long-lived sigma*(OCN) shape resonance and the little sigma* admixture into the pi* resonances located on the cyanate group. The present results thus indicate 5-SCNU as a more promising radiosensitizer at sub-excitation energies.

JOURNAL OF CHEMICAL PHYSICS 147[21], 214310, 2017. DOI: 10.1063/1.5007050

[P385-2017] "Vibration and Magnetic Field Sensing Using a Long-Period Grating"

Nascimento, I. M.; **Chesini, G.*;** Baptista, J. M.; **Cordeiro, C. M. B.***; Jorge, P. A. S.

A long-period grating (LPG) written on a standard single mode fiber is investigated as a fiber optic sensor for vibration and magnetic field sensing. It is demonstrated the high sensitivity of the device to applied curvature and the possibility to monitor vibration in a wide range of frequencies from 30 Hz to 2000 Hz.

The system was tested using intensity-based interrogation scheme, providing a frequency discrimination of 913 mHz. The goal of these tests was to evaluate the sensor as a passive vibration monitor in the detection of changes in resonant vibration frequencies of support infrastructures can provide information on its degradation. Furthermore, taking advantage of the intrinsic sensitivity to micro strain, alternating magnetic fields were also measured using an intensity-based interrogation scheme by coupling a Terfenol-D magnetostrictive rod to a pre-strained LPG sensor, providing a resolution below 5.61 mu T-rms/root Hz from 1.22 mT(rms) up to 2.53 mT(rms).

IEEE SENSORS JOURNAL 17[20], 6615-6621, 2017. DOI: 10.1109/JSEN.2017.2743112

[P386-2017] "Constraints on anomalous Higgs boson couplings using production and decay information in the four--lepton final state"

Sirunyan, A. M.; Turnasyan, A.; Adam, W.; **Chinellato, J. A.*; Tonelli Manganote, E. J.***; et al.
CMS Collaboration

A search is performed for anomalous interactions of the recently discovered Higgs boson using matrix element techniques with the information from its decay to four leptons and from associated Higgs boson production with two quark jets in either vector boson fusion or associated production with a vector boson. The data were recorded by the CMS experiment at the LHC at a center-of-mass energy of 13 TeV and correspond to an integrated luminosity of 38.6 fb(-1). They are combined with the data collected at center-of-mass energies of 7 and 8 TeV, corresponding to integrated luminosities of 5.1 and 19.7 fb(-1), respectively. All observations are consistent with the expectations for the standard model Higgs boson.

PHYSICS LETTERS B 775, 1-24, 2017. DOI: 10.1016/j.physletb.2017.10.021

[P387-2017] "What measurements of neutrino neutral current events can reveal"

Gandhi, R.; Kayser, B.; **Prakash, S.*;** Roy, S.

We show that neutral current (NC) measurements at neutrino detectors can play a valuable role in the search for new physics. Such measurements have certain intrinsic features and advantages that can fruitfully be combined with the usual well-studied charged lepton detection channels in order to probe the presence of new interactions or new light states. In addition to the fact that NC events are immune to uncertainties in standard model neutrino mixing and mass parameters, they can have small matter effects and superior rates since all three flavours participate. We also show, as a general feature, that NC measurements provide access to different combinations of CP phases and mixing parameters compared to CC measurements at both long and short baseline experiments. Using the Deep Underground Neutrino Experiment (DUNE) as an illustrative setting, we demonstrate the capability of NC measurements to break degeneracies arising in CC measurements, allowing us, in principle, to distinguish between new physics that violates three flavour unitarity and that which does not. Finally, we show that NC measurements can enable us to restrict new physics parameters that are not easily constrained by CC measurements.

JOURNAL OF HIGH ENERGY PHYSICS 11, 202, 2017. DOI: 10.1007/JHEP11(2017)202

Eventos publicados 2017

[P388-2017] "3D Printed Microstructured Optical Fibers"

Marques, T. H. R.*; Lima, B. M.*; Osorio, J. H.*; da Silva, L. E.*; Cordeiro, C. M. B.*
IEEE

In this investigation we report, to the best of our knowledge, the first realization of air-core optical fibers obtained by drawing a 3D printed preform. Two different optical fibers are presented. Descriptions on the preform preparation and fiber drawing are provided, and our preliminary results are presented.

17th SBMO/IEEE MTT-S International Microwave and Optoelectronics Conference (IMOC), AUG 27-30, 2017, Aguas de Lindoia, BRAZIL.

2017 SBMO/IEEE MTT-S INTERNATIONAL MICROWAVE AND OPTOELECTRONICS CONFERENCE (IMOC), 2017.

[P389-2017] "Characterization of nonlinear carrier dynamics in silicon strip nanowaveguides"

Aldaya, I.*; Dainese, P.*; Gil-Molina, A.; Pita, J. L.; **Fragnito, H. L.***
IEEE

Nonlinear carrier recombination dynamics is characterized in a 450 nm x 220 nm silicon nanowire by employing a time-resolved pump-and-probe experiment. Our results show that the recombination rate is faster at the early stages of the decay as compared to the final stages, in agreement with trap-assisted mechanism. We have also demonstrated that by operating at high carrier density, faster excess carrier generation and recombination can be obtained, which we have used to improve the speed of an all-optical FCA based silicon switch from about 7 to 1 ns.

17th SBMO/IEEE MTT-S International Microwave and Optoelectronics Conference (IMOC), AUG 27-30, 2017, Aguas de Lindoia, BRAZIL.

2017 SBMO/IEEE MTT-S INTERNATIONAL MICROWAVE AND OPTOELECTRONICS CONFERENCE (IMOC), 2017.

[P390-2017] "Exploring THz Hollow-Core Fiber Designs Manufactured by 3D Printing"

Cruz, A. L. S.; Franco, M. A. R.; **Cordeiro, C. M. B.*; Rodrigues, G. S.*; Osorio, J. H.*; da Silva, L. E.***
IEEE

In this paper we demonstrate the terahertz propagation characteristics of 3D printed hollow core fibers with inner capillaries. The fibers were numerically characterized using a beam propagation method software. The guidance is supported by antiresonant effect and the spectral transmission was evaluated until 1.6 THz. Special designs were proposed exploring the versatility of 3D printing technique. The potential application of these THz waveguides as a refractometer is presented.

17th SBMO/IEEE MTT-S International Microwave and Optoelectronics Conference (IMOC), AUG 27-30, 2017, Aguas de Lindoia, BRAZIL.

2017 SBMO/IEEE MTT-S INTERNATIONAL MICROWAVE AND OPTOELECTRONICS CONFERENCE (IMOC), 2017.

[P391-2017] "Nano-antennas on tapered fiber: a new and flexible approach"

Khaleque, A.; Hattori, H. T.; **Osorio, J. H.*; Cordeiro, C. M. B.***; Franco, M. A. R.
IEEE

This paper proposes a new and flexible approach to control the electric field enhancement of bow-tie nano-antennas by integrating them on the lateral of a similar to 9 mu m tapered optical fiber. The device may find applications in bio-sensing and imaging.

Conference on Lasers and Electro-Optics Pacific Rim (CLEO--PR), JUL 31-AUG 04, 2017, Singapore, SINGAPORE.

2017 CONFERENCE ON LASERS AND ELECTRO-OPTICS PACIFIC RIM (CLEO-PR), 2017.

Artigos publicados 2018

[P001-2018] "Atomic Layered Titanium Sulfide Quantum Dots as Electrocatalysts for Enhanced Hydrogen Evolution Reaction"

Liu, Y.; Liang, C. L.; Wu, J. J.; Sharifi, T.; Xu, H.; Nakanishi, Y.; Yang, Y. C.; **Woellne, C. F.*;** Aliyan, A.; Marti, A. A.; Xie, B. H.; Vajtai, R.; Yang, W.; Ajayan, P. M.

The overall electrocatalytic activity toward hydrogen evolution reaction for layered transition metal dichalcogenides is governed by their intrinsic activity, the corresponding density of active sites, and the electron transfer resistance. Here, nanoengineering strategies to scale down both the lateral size and thickness of layered 1T-TiS2 powder to quantum dots (QDs) by bath sonication and probing sonication incision are employed. Uniform lateral size of 3-6 nm in the resulting QDs enhances the density of edge sites while the atomic layer thickness (1-2 nm) facilitates the electron transfer from the substrate to the edge sites. The obtained TiS2 QDs exhibit superior hydrogen evolution reaction activity over TiS2 nanosheets and MoS2 QDs prepared by the same method. The turnover frequency of TiS2 QDs with a small loading of 0.7 ng cm(-2) in an optimal deposition on electrode reached approximate to 2.0 s(-1) at an overpotential of -0.2 V versus RHE, several orders of magnitude higher than TiS2 nanosheets (0.01 s(-1)) and MoS2 QDs (0.07 s(-1)).

ADVANCED MATERIALS INTERFACES 5[1], 1700895, 2018. DOI: 10.1002/admi.201700895

[P002-2018] "Can graph metrics be used for EEG-BCIs based on hand motor imagery?"

Stefano, C .A.*; Attux, R.*; Castellano, G.*

The study of motor imagery (MI) has been a subject of great interest within the brain-computer interface (BCI) community. Several approaches have been proposed to solve the problem of classifying cerebral responses due to MI, mostly based on the power spectral density of the mu and beta bands; however, no optimum manner of proceeding through the fundamental steps of a MI-BCI has yet been established. In this work, we explored a relatively novel approach regarding feature generation for a MI-BCI by assuming that functional connectivity patterns of the brain are altered during hand MI. We modelled interactions among EEG electrodes by a graph, extracted metrics from it during left and right hand MI from eight subjects and classified the signals using commonly employed techniques in the BCI community (LDA and SVM). We also compared this approach to the more established method of using the signal power spectral density as the classifier features. With the graph method, we confirmed that only specific electrodes provide relevant information for data classification. A first approach provided maximum average classification rates across all subjects for the graph method of 86% for the mu band and 87% for the beta band. For the PSD method, average rates were of 98% and 99% for the mu and beta bands, respectively. However, a much larger number of features was needed: (130 44) and (273 89) for the mu and beta bands, respectively. Aiming to reproduce these rates using the graph method, pairwise inputs combinations of graph metrics were tested. They proved to be sufficient to obtain essentially the same classification accuracy rates, but with a considerably smaller number of features - about 60 features, for both bands. We thus conclude that the graph method is a feasible option for classification of hand MI signals.

BIOMEDICAL SIGNAL PROCESSING AND CONTROL 40, 359-365, 2018. DOI: 10.1016/j.bspc.2017.09.026

[P003-2018] "Chemical Abundance Analysis of Three alpha--poor, Metal-poor Stars in the Ultrafaint Dwarf Galaxy Horologium I"

Nagasawa, D. Q.; Marshall, J. L.; Li, T. S.; **Sobreira, F.***; et al.

We present chemical abundance measurements of three stars in the ultrafaint dwarf galaxy Horologium I, a Milky Way satellite discovered by the Dark Energy Survey. Using high--resolution spectroscopic observations, we measure the metallicity of the three stars, as well as abundance ratios of several alpha-elements, iron-peak elements, and neutron--capture elements. The abundance pattern is relatively consistent among all three stars, which have a low average metallicity of [Fe/H]similar to -2.6 and are not alpha-enhanced ([alpha/Fe] similar to 0.0). This result is unexpected when compared to other low-metallicity stars in the Galactic halo and other ultrafaint dwarfs and suggests the possibility of a different mechanism for the enrichment of Hor I compared to other satellites. We discuss possible scenarios that could lead to this observed nucleosynthetic signature, including extended star formation, enrichment by a Population III supernova, and or an association with the Large Magellanic Cloud.

ASTROPHYSICAL JOURNAL 852[2], 99, 2018. DOI: 10.3847/1538-4357/aaa01d

[P004-2018] "COSMOGRAIL: the COSmological MOnitoring of GRAvItational Lenses XVI. Time delays for the quadruply imaged quasar DES J0408-5354 with high-cadence photometric monitoring"

Courbin, F.; Bonvin, V.; Buckley-Geer, E.; **Sobreira, F.*;** et al.

We present time-delay measurements for the new quadruple imaged quasar DES J0408-5354, the first quadruple imaged quasar found in the Dark Energy Survey (DES). Our result is made possible by implementing a new observational strategy using almost daily observations with the MPIA 2.2 m telescope at La Silla observatory and deep exposures reaching a signal-to--noise ratio of about 1000 per quasar image. This data quality allows us to catch small photometric variations (a few mmag rms) of the quasar, acting on temporal scales much shorter than microlensing, and hence making the time delay measurement very robust against microlensing. In only seven months we very accurately measured one of the time delays in DES J0408-5354: Delta t(AB) = -112.1 +/- 2.1 days (1.8%) using only the MPIA 2.2 m data. In combination with data taken with the 1.2 m Euler Swiss telescope, we also measured two delays involving the D component of the system Delta t(AD) = -155.5 +/- 12.8 days (8.2%) and Delta t(BD) = -42.4 +/- 17.6 days (41%), where all the error bars include systematics. Turning these time delays into cosmological constraints will require deep Hubble Space Telescope (HST) imaging or ground-based adaptive optics (AO), and information on the velocity field of the lensing galaxy.

ASTRONOMY & ASTROPHYSICS 609, A71, 2018. DOI: 10.1051/0004-6361/201731461

[P005-2018] "Dosimetric evaluation of radionuclides for VCAM-1-targeted radionuclide therapy of early brain metastases"

Falzone, N.; Ackerman, N. L.; **Rosales, L. D.*; Bernal, M. A.***; Liu, X. X.; Peeters, S. G. J. A.; Soto, M. S.; Corroyer-Dulmont, A.; Bernaudin, M.; Grimoin, E.; Touzani, O.; Sibson, N. R.; Vallis, K. A.

Brain metastases develop frequently in patients with breast cancer, and present a pressing therapeutic challenge. Expression of vascular cell adhesion molecule 1 (VCAM-1) is upregulated on brain endothelial cells during the early stages of metastasis and provides a target for the detection and treatment of early brain metastases. The aim of this study was to use a model of early brain metastasis to evaluate the efficacy of a-emitting radionuclides, Tb-149, At-211, Pb-212, Bi-213 and Ac-225; beta-emitting radionuclides, Y-90, Tb-161 and Lu-177; and Auger electron (AE)-emitters Ga-67, Zr-89, In-111 and I-124, for targeted radionuclide therapy (TRT). METHODS: Histologic sections and two photon microscopy of mouse brain parenchyma were used to inform a cylindrical vessel geometry using the Geant4 general purpose Monte Carlo (MC) toolkit with the Geant4--DNA low energy physics models. Energy deposition was evaluated as a radial function and the resulting phase spaces were superimposed on a DNA model to estimate double-strand break (DSB) yields for representative beta- and alpha-emitters, Lu-177 and Pb-212. Relative biological effectiveness (RBE) values were determined by only evaluating DNA damage due to physical interactions. RESULTS: Lu-177 produced 2.69 +/- 0.08 DSB per GbpGy, without significant variation from the lumen of the vessel to a radius of 100 mu m. The DSB yield of Pb-212 included two local maxima produced by the 6.1 MeV and 8.8 MeV alpha--emissions from decay products, Bi-212 and Po-212, with yields of 7.64 +/- 0.12 and 9.15 +/- 0.24 per GbpGy, respectively. Given its higher DSB yield Pb-212 may be more effective for short range targeting of early micrometastatic lesions than Lu-177. CONCLUSION: MC simulation of a model of early brain metastases provides invaluable insight into the potential efficacy of alpha-, beta- and AE-emitting radionuclides for TRT. Pb-212, which has the attributes of a theranostic radionuclide since it can be used for SPECT imaging, showed a favorable dose profile and RBE.

THERANOSTICS 8[1], 292-303, 2018. DOI: 10.7150/thno.22217

[P006-2018] "Electronic Transport and Raman Spectroscopy Characterization in Ion-Implanted Highly Oriented Pyrolytic Graphite"

de Jesus, R. F.; Turatti, A. M.; **Camargo, B. C.*; da Silva, R. R.*; Kopelevich, Y.***; Behar, M.; Balzaretti, N. M.; Gusmao, M. A.; Pureur, P.

We report on Raman spectroscopy, temperature-dependent in--plane resistivity, and in-plane magnetoresistance experiments in highly oriented pyrolytic graphite (HOPG) implanted with As and Mn. A pristine sample was also studied for comparison. Two different fluences were applied, and . The implantations were carried out with 20 keV ion energy at room temperature. The Raman spectroscopy results reveal the occurrence of drastic changes of the HOPG surface as a consequence of the damage caused by ionic implantation. For the higher dose, the complete amorphization limit is attained. The resistivity and magnetoresistance results were obtained placing electrical contacts on the irradiated sample surface. Owing to the strong anisotropy of HOPG, the electrical current propagates mostly near the implanted surface. Shubnikov-de Haas (SdH) oscillations were observed in the magnetoresistance at low temperatures. These results allow the extraction of the fundamental SdH frequencies and the carriers' effective masses. In general, the resistivity and magnetoresistance results are consistent with those obtained from Raman measurements. However, one must consider that the electrical conduction in our samples occurs as in a parallel association of a largely resistive thin sheet at the surface strongly modified by disorder with a thicker layer where damage produced by implantation is less severe. The SdH oscillations do not hint to significant changes in the carrier density of HOPG.

JOURNAL OF LOW TEMPERATURE PHYSICS 190[3-4], 141-153, 2018. DOI: 10.1007/s10909-017-1825-8

[P007-2018] "Engineered nonlinear materials using gold nanoantenna array"

Drachev, V. P.; Kildishev, A. V.; Borneman, J. D.; Chen, K. P.; Shalaev, V. M.; Yamnitskiy, K.; Norwood, R. A.; Peyghambarian, N.; Marder, S. R.; **Padilha, L. A.***; Webster, S.; Ensley, T. R.; Hagan, D. J.; Van Stryland, E. W.

Gold dipole nanoantennas embedded in an organic molecular film provide strong local electromagnetic fields to enhance both the nonlinear refractive index (n(2)) and two-photon absorption (2PA) of the molecules. An enhancement of 53x for 2PA and 140x for nonlinear refraction is observed for BDPAS (4,4'-bis(diphenylamino) stilbene) at 600 nm with only 3.7% of gold volume fraction. The complex value of the third--order susceptibility enhancement results in a sign change of n(2) for the effective composite material relative to the pure BDPAS film. This complex nature of the enhancement and the tunability of the nanoantenna resonance allow for engineering the effective nonlinear response of the composite film.

SCIENTIFIC REPORTS 8, 780, 2018. DOI: 10.1038/s41598-017-19066-3

[P008-2018] "Forward Global Photometric Calibration of the Dark Energy Survey"

Burke, D. L.; Rykoff, E. S.; Allam, S.; **Sobreira, F.***; et al.
DES Collaboration

Many scientific goals for the Dark Energy Survey (DES) require the calibration of optical/NIR broadband b = grizY photometry that is stable in time and uniform over the celestial sky to one percent or better. It is also necessary to limit to similar accuracy systematic uncertainty in the calibrated broadband magnitudes due to uncertainty in the spectrum of the source. Here we present a "Forward Global Calibration Method (FGCM)" for photometric calibration of the DES, and we present results of its application to the first three years of the survey (Y3A1). The FGCM combines data taken with auxiliary instrumentation at the observatory with data from the broadband survey imaging itself and models of the instrument and atmosphere to estimate the spatial and time dependences of the passbands of individual DES survey exposures. "Standard" passbands that are typical of the passbands encountered during the survey are chosen. The passband of any individual observation is combined with an estimate of the source spectral shape to yield a magnitude m(b)(std) in the standard system. This " chromatic correction" to the standard system is necessary to achieve subpercent calibrations and in particular, to resolve ambiguity between the broadband brightness of a source and the shape of its SED. The FGCM achieves a reproducible and stable photometric calibration of standard magnitudes m(b)(std) of stellar sources over the multiyear Y3A1 data sample with residual random calibration errors of sigma = 6-7 mmag per exposure. The accuracy of the calibration is uniform across the 5000 deg(2) DES footprint to within sigma = 7 mmag. The systematic uncertainties of magnitudes in the standard system due to the spectra of sources are less than 5 mmag for main-sequence stars with 0.5 < g-i < 3.0.

ASTRONOMICAL JOURNAL 155[1], 41, 2018. DOI: 10.3847/1538-3881/aa9f22

[P009-2018] "High pressure studies on bis(L-histidinate) nickel(II) monohydrate"

Maia, J. R.; Lima, J. A., Jr.; Freire, P. T. C.; Melo, F. E. A.; de Menezes, A. S.; Remedios, C. M. R.; **Cardoso, L. P.***

Raman spectra of bis (L-histidinate)nickel(11) monohydrate crystal were obtained for pressures up to 9.5 GPa. Our results show the disappearance of some of the Raman modes and the appearance of other modes. These modifications evidence that the sample undergoes phase transitions at around 0.8 and 3.2 GPa. The role played by the Ni ions and hydrogen bonds in the dynamics of the phase transitions is discussed. Under decompression, down to atmospheric pressure, the original Raman spectra are recovered, showing that both phase transitions are fully reversible.

SPECTROCHIMICA ACTA PART A-MOLECULAR AND BIOMOLECULAR SPECTROSCOPY 189, 258-264, 2018. DOI: 10.1016/j.saa.2017.08.040

[P010-2018] "How Many Kilonovae Can Be Found in Past, Present, and Future Survey Data Sets?"

Scolnic, D.; Kessler, R.; Brout, D.; **Sobreira, F*.**; et al.
DES Collaboration

The discovery of a kilonova (KN) associated with the Advanced LIGO (aLIGO)/Virgo event GW170817 opens up new avenues of multi-messenger astrophysics. Here, using realistic simulations, we provide estimates of the number of KNe that could be found in data from past, present, and future surveys without a gravitational-wave trigger. For the simulation, we construct a spectral time-series model based on the DES-GW multi-band light curve from the single known KN event, and we use an average of BNS rates from past studies of 103Gpc(-3) yr(-1), consistent with the one event found so far. Examining past and current data sets from transient surveys, the number of KNe we expect to find for ASAS-SN, SDSS, PS1, SNLS, DES, and SMT is between 0 and 0.3. We predict the number of detections per future survey to be 8.3 from ATLAS, 10.6 from ZTF, 5.5/69 from LSST (the Deep Drilling/Wide Fast Deep), and 16.0 from WFIRST. The maximum redshift of KNe discovered for each survey is z = 0.8 for WFIRST, z = 0.25 for LSST, and z = 0.04 for ZTF and ATLAS. This maximum redshift for WFIRST is well beyond the sensitivity of aLIGO and some future GW missions. For the LSST survey, we also provide contamination estimates from Type Ia and core-collapse supernovae: after light curve and template-matching requirements, we estimate a background of just two events. More broadly, we stress that future transient surveys should consider how to optimize their search strategies to improve their detection efficiency and to consider similar analyses for GW follow-up programs.

ASTROPHYSICAL JOURNAL LETTERS 852[1], L3, 2018. DOI: 10.3847/2041-8213/aa9d82

[P011-2018] "Insight into dual-modality of triply doped magnetic-luminescent iron-oxide/NaGdF4:RE3+ (RE = Ce, Tb, Dy) nanoparticles"

Shrivastava, N.; Rocha, U.; **Muraca, D.***; Silva, W.; Jacinto, C.; Kumar, R.; Sharma, S. K.

Green emitting iron-oxide@NaGdF4:RE3+ (RE = 5%Ce, 5%Tb, 5%Dy) nanoparticles have been synthesized using microwave assisted solvothermal method. The Rietveld analysis of powder X-ray diffraction and high-resolution transmission electron microscopy provides an average crystallite size (similar to 20 nm) and the hexagonal crystal structure. Magnetic hysteresis loops at 300 K display superparamagnetic behavior along with paramagnetic feature for the reference NaGdF4:RE3+, further validated through magnetization versus temperature curves taken in an external magnetic field of 100 Oe. The photoluminescence investigation of the nanoparticles, suggest a down-converting energy transfer. The excitation spectra consist of a dominant broad band at around 254 nm due to Ce3+(4f-5d) along with f-f transitions due to Gd3+, Tb3+ and Dy3+ ions. The strong emission color lines due to characteristic transitions of Tb3+ (D-5(4) -> F-7(J), J = 6-3), and Dy3+ (F-4(9/2)-H-6(15/2), H-6(13/2)), were observed. The luminescence quenching in iron-oxide/NaGdF4: RE3+ through leakage path provided by iron-oxide to excite electrons has been confirmed and explained by comparing the time decay analysis.

MATERIALS LETTERS 213, 358-361, 2018. DOI: 10.1016/j.matlet.2017.11.037

[P012-2018] "Insights on the mechanism of water-alcohol separation in multilayer graphene oxide membranes: Entropic versus enthalpic factors"

Borges, D. D.*; Woellner, C. F.*; Autreto, P. A. S.; **Galvao, D. S.***

Experimental evidence has shown that graphene oxide (GO) can be impermeable to liquids, vapors and gases, while it allows a fast permeation of water molecules. Theoretical studies to understand the filtration mechanisms come mostly from water desalination, while very few works have been dedicated to alcohol dehydration. In this work, we have investigated the molecular level mechanism underlying the alcohol/water separation inside GO membranes. A series of Molecular Dynamics and Grand-Canonical Monte Carlo simulations were carried out to probe the ethanol/water and methanol/water separation through GO membranes composed of multiple layered graphene-based films with different interlayer distance values and number of oxygen-containing functional groups. Our results show that the size exclusion and membrane affinities are not sufficient to explain the selectivity. Besides that, the favorable water molecular arrangement inside GO 2D-channels forming a robust H-bond network and the fast water permeation are crucial for an effective separation mechanism. In other words, the separation phenomenon is not only governed by membrane affinities (enthalpic mechanisms) but mainly by the geometry and size factors (entropic mechanisms). Our findings are consistent with the available experimental data and contribute to clarify important aspects of the separation behavior of confined alcohol/ water in GO membranes.

CARBON 127, 280-286, 2018. DOI: 10.1016/j.carbon.2017.11.020

[P013-2018] "Jansen-MIDAS: A multi-level photomicrograph segmentation software based on isotropic undecimated wavelets"

de Siqueira, A. F.*; Cabrera, F. C.; **Nakasuga, W. M.***; Pagamisse, A.; Job, A. E.

Image segmentation, the process of separating the elements within a picture, is frequently used for obtaining information from photomicrographs. Segmentation methods should be used with reservations, since incorrect results can mislead when interpreting regions of interest (ROI). This decreases the success rate of extra procedures. Multi-Level Starlet Segmentation (MLSS) and Multi-Level Starlet Optimal Segmentation (MLSOS) were developed to be an alternative for general segmentation tools. These methods gave rise to Jansen-MIDAS, an open-source software. A scientist can use it to obtain several segmentations of hers/his photomicrographs.

It is a reliable alternative to process different types of photomicrographs: previous versions of Jansen-MIDAS were used to segment ROI in photomicrographs of two different materials, with an accuracy superior to 89%.

MICROSCOPY RESEARCH AND TECHNIQUE 81[1], 22-32, 2018. DOI: 10.1002/jemt.22952

[P014-2018] "Magnetic and magnetocaloric properties in Gd1-yPryNi2 compounds"

Alho, B. P.; Lopes, P. H. O.; Ribeiro, P. O.; Alvarenga, T. S. T.; Nobrega, E. P.; de Sousa, V. S. R.; Carvalho, A. M. G.; Caldas, A.; Tedesco, J. C. G.; **Coelho, A. A.***; de Oliveira, N. A.; von Ranke, P. J.

In this work, we report the magnetic and magnetocaloric properties of the Gd1-yPryNi2 compounds from both experimental and theoretical points of view. It is worth noting that this series shows a variety of magnetic arrangements depending on the Pr concentration, including paramagnetism, ferrimagnetism and ferromagnetism. Our experimental work consists of the systematic analysis of the magnetic properties of the compounds with y = 0.0, 0.25, 0.5, 0.75 and 1.0, which includes temperature and magnetic field dependence of the magnetization, heat capacity and isothermal entropy change obtained by isothermal magnetization curves. Also, we developed a model Hamiltonian, which takes into account the exchange interactions among Gd-Gd, Gd-Pr and Pr-Pr ions, the Zeeman interaction for both ions and the crystalline electrical field interaction for the Pr ions. We systematically investigated the magnetic properties of the series and obtained a good agreement when compared with our experimental data.

JOURNAL OF MAGNETISM AND MAGNETIC MATERIALS 449[308-312, 2018. DOI: 10.1016/j.jmmm.2017.10.044

[P015-2018] "Multiscale Geometric Design Principles Applied to 3D Printed Schwarzites"

Sajadi, S. M.; Owuor, P. S.; Schara, S.; **Woellner, C. F.*; Rodrigues, V***.; Vajtai, R.; Lou, J.; **Galvao, D. S.***; Tiwary, C. S.; Ajayan, P. M.

Schwartzites are 3D porous solids with periodic minimal surfaces having negative Gaussian curvatures and can possess unusual mechanical and electronic properties. The mechanical behavior of primitive and gyroid schwartzite structures across different length scales is investigated after these geometries are 3D printed at centimeter length scales based on molecular models. Molecular dynamics and finite elements simulations are used to gain further understanding on responses of these complex solids under compressive loads and kinetic impact experiments. The results show that these structures hold great promise as high load bearing and impact-resistant materials due to a unique layered deformation mechanism that emerges in these architectures during loading. Easily scalable techniques such as 3D printing can be used for exploring mechanical behavior of various predicted complex geometrical shapes to build innovative engineered materials with tunable properties.

ADVANCED MATERIALS 30[1], 1704820, 2018. DOI: 10.1002/adma.201704820

[P016-2018] "Neutrino Oscillations within the Induced Gravitational Collapse Paradigm of Long Gamma-Ray Bursts"

Becerra, L.; **Guzzo, M. M.*; Rossi-Torres, F.*;** Rueda, J. A.; Ruffini, R.; Uribe, J. D.

The induced gravitational collapse paradigm of long gamma--ray bursts associated with supernovae (SNe) predicts a copious neutrino-antineutrino (nu(nu) over bar) emission owing to the hypercritical accretion process of SN ejecta onto a neutron star (NS) binary companion. The neutrino emission can reach luminosities of up to 10(57) MeV. s(-1), mean neutrino energies of 20 MeV, and neutrino densities of 10(31) cm(-3). Along their path from the vicinity of the NS surface outward, such neutrinos experience flavor transformations dictated by the neutrino-to--electron-density ratio. We determine the neutrino and electron on the accretion zone and use them to compute the neutrino flavor evolution. For normal and inverted neutrino mass hierarchies and within the two-flavor formalism (nu(e)nu(x)), we estimate the final electronic and nonelectronic neutrino content after two oscillation processes: (1) neutrino collective effects due to neutrino self-interactions where the neutrino density dominates, and (2) the Mikheyev-Smirnov-Wolfenstein effect, where the electron density dominates. We find that the final neutrino content is composed by similar to 55% (similar to 62%) of electronic neutrinos, i.e., nu(e) + (nu) over bar (e), for the normal (inverted) neutrino mass hierarchy. The results of this work are the first step toward the characterization of a novel source of astrophysical MeV neutrinos in addition to core-collapse SNe and, as such, deserve further attention.

ASTROPHYSICAL JOURNAL 852[2], 120, 2018. DOI: 10.3847/1538-4357/aaa296

[P017-2018] "Search for resonant and nonresonant Higgs boson pair production in the b(b)over-barl nu l nu final state in proton-proton collisions at root s=13 TeV"

Sirunyan, A. M.; Tumasyan, A.; Adam, W.; **Chinellato, J. A.*;** et al.
CMS Collaboration

Searches for resonant and nonresonant pair-produced Higgs bosons (HH) decaying respectively into l nu l nu, through either W or Z bosons, and b (b) over bar are presented. The analyses are based on a sample of proton-proton collisions at root s = 13 TeV, collected by the CMS experiment at the LHC, corresponding to an integrated luminosity of 35.9 fb(-1). Data and predictions from the standard model are in agreement within uncertainties. For the standard model HH hypothesis, the data exclude at 95% confidence level a product of the production cross section and branching fraction larger than 72 fb, corresponding to 79 times the standard model prediction. Constraints are placed on different scenarios considering anomalous couplings, which could affect the rate and kinematics of HH production. Upper limits at 95% confidence level are set on the production cross section of narrow-width spin-0 and spin-2 particles decaying to Higgs boson pairs, the latter produced with minimal gravity-like coupling.

JOURNAL OF HIGH ENERGY PHYSICS [1], 054, 2018. DOI: 10.1007/JHEP01(2018)054

[P018-2018] "Separating the influence of electric charges in magnetic force microscopy images of inhomogeneous metal samples"

Arenas, M. P.; Lanzoni, E. M.; Pacheco, C. J.; Costa, C. A. R.; Eckstein, C. B.; de Almeida, L. H.; Rebello, J. M. A.; **Deneke, C. F.***; Pereira, G. R.

In this study, we investigate artifacts arising from electric charges present in magnetic force microscopy images. Therefore, we use two austenitic steel samples with different microstructural conditions. Furthermore, we examine the influence of the surface preparation, like etching, in magnetic force images. Using Kelvin probe force microscopy we can quantify the charges present on the surface.

Our results show that electrical charges give rise to a signature in the magnetic force microscopy, which is indistinguishable from a magnetic signal. Our results on two differently aged steel samples demonstrate that the magnetic force microscopy images need to be interpreted with care and must be corrected due to the influence of electrical charges present. We discuss three approaches, how to identify these artifacts - parallel acquisition of magnetic force and electric force images on the same position, sample surface preparation to decrease the presence of charges and inversion of the magnetic polarization in two succeeding measurement.

JOURNAL OF MAGNETISM AND MAGNETIC MATERIALS 446, 239-244, 2018. DOI: 10.1016/j.jmmm.2017.09.041

[P019-2018] "The ALICE Transition Radiation Detector: Construction, operation, and performance"

Acharya, S.; Adam, J.; Adamova, D.; **Albuquerque, D. S. D.*; Chinellato, D. D.*; De Souza, R. D.; Takahashi, J.***; et al.
ALICE Collaboration

The Transition Radiation Detector (TRD) was designed and built to enhance the capabilities of the ALICE detector at the Large Hadron Collider (LHC). While aimed at providing electron identification and triggering, the TRD also contributes significantly to the track reconstruction and calibration in the central barrel of ALICE. In this paper the design, construction, operation, and performance of this detector are discussed. A pion rejection factor of up to 410 is achieved at a momentum of 1 GeV/c in p-Pb collisions and the resolution at high transverse momentum improves by about 40% when including the TRD information in track reconstruction. The triggering capability is demonstrated both for jet, light nuclei, and electron selection.

NUCLEAR INSTRUMENTS & METHODS IN PHYSICS RESEARCH SECTION A-ACCELERATORS SPECTROMETERS DETECTORS AND ASSOCIATED EQUIPMENT 881, 88-127, 2018. DOI:10.1016/j.nima.2017.09.028

[P020-2018] "Theoretical evaluation of chemical substitutions along the main chain of poly(3-hexylthienylene-vinylene) for solar cell applications"

Roldao, J. C.; **Oliveira, E. F.***; Sato, F.; Lavarda, F. C.

In order to improve the efficiency of bulk-heterojunction organic solar cells, one can try to optimize the active layer through the use of new materials that provide improvements in the parameters that influence the final efficiency of a device. The use of chemical substitutions in organic materials already used in these devices seems to be an efficient methodology to obtain new materials with better intrinsic properties. Based on this idea, in this work is investigated theoretically, by methods of electronic structure calculation, a set of 143 poly(3-hexylthienylene-vinylene) (P3HTV) derivatives for application in active layers of organic solar cells as electron donor materials; the chemical modifications were performed on the thiophene ring and the vinyl segment of P3HTV. The results show that it is possible to obtain several new derivatives with better optical and electronic properties than those of P3HTV. The derivative substituted with trifluoromethyl on the vinyl segment is one of the most promising for use in active layers, when combined with phenyl-C61-butyric-acid--methyl-ester as electron acceptor material. An equation to predict the electronic properties of P3HTV derivatives when using more than one chemical substitution is also proposed, which is corroborated by the theoretical calculations.

POLYMER INTERNATIONAL 67[2], 197-203, 2018. DOI: 10.1002/pi.5496

***Autores da comunidade IFGW**
Fonte: Web of Science on-line.

Patentes 2017

[Pa005-2017] "Nanopartículas com Propriedades Ópticas de Fluorescência e Uso"

Marcelo Giannini, Jorge Rodrigo Soto Montero, Eduardo David Martinez, Ali Francisco Garcia Flores, Ailla Carla Rocha Acosta Lancellotti, Guilherme Gorgen Lesseux, Rafael Rocha Pacheco, Frederick Allen Rueggeberg, Carlos Rettori, Ricardo Rodrigues Urbano

Número da Patente ou Registro: Agência INOVA: BR 10 2017 027647 3
Tipo: Patente de Invenção
Mês/Ano de Conclusão: 12/2017 - INPI/BBRASIL

[Pa006-2017] "Método para acessar e encher lateralmente a estrutura interna de fibras ópticas micro-estruturadas e fibras ópticas com acesso lateral assim obtidas"

Cristiano Monteiro de Barros Cordeiro, Carlos Henrique de Brito Cruz, Christiano José Santiago de Matos

Número da Patente ou Registro: Agência INOVA: PI 0701339-6
Tipo: Patente de Invenção
Mês/Ano de Conclusão: 12/2017 - INPI/BBRASIL

[Pa007-2017] "Biossensor Óptico Integrado, Método de Detecção E Usos do Biossensor"

Newton Cesario Frateschi, Mário César Mendes Machado de Souza, André Luís Morás Junior, Luís Alberto Mijam Barêa

Número da Patente ou Registro: Agência INOVA: BR 10 2017 027015 7
Tipo: Patente de Invenção
Mês/Ano de Conclusão: 12/2017 - INPI/BBRASIL

Fonte: SIPEX - Sistema de Informação de Pesquisa e Extensão da Unicamp.

Defesas de Dissertações

[D001-2018] "Effects of multi-parton interactions in high--multiplicity proton-proton collisions"
Aluno: Renan Teixeira Acconcia
Orientador: Prof. Dr. David Dobrigkeit Chinellato
Data: 29/01/2018

Defesas de Teses

[T001-2018] "Optical gain medium incorporation into semiconductor optomechanical cavities"
Aluno: Débora Princepe
Orientador: Prof. Dr. Newton Cesario Frateschi
Data: 30/01/2018

[T002-2018] "Efeito da Simetria de Bose no Cálculo de Energias em Sistemas Formados por Átomos de ^{4}He nos métodos Variacional e Difusão Monte Carlo"
Aluno: Elkin Jezzid Rugeles Vargas
Orientador: Prof. Dr. Silvio Antonio S. Vitiello
Data: 30/01/2018

[T003-2018] "Estudo da Interface TiN/Silicio Cristalino por Espectroscopia de Electrons Fotoemitidos por Raios X (XPS)"
Aluno: Vinicius Gabriel Antunes
Orientador: Prof. Dr. Fernando Alvarez
Data: 30/01/2018

[T004-2018] "Muon detection with AMIGA at the Pierre Auger Observatory"
Aluno: Bruno Daniel
Orientador: Prof. Dr. Ernesto Kemp
Data: 22/02/2018

[T005-2018] "Estudy of Impedances and Collective Instabilities applied to Sirius"
Aluno: Fernando Henrique de Sá
Orientador: Prof. Dr. Antonio Rubens Britto de Castro
Data: 27/02/2018

Fonte: Portal IFGW/Pós-graduação - Agenda de Colóquios, Defesas e Seminários.
Disponível em: http://portal.ifi.unicamp.br/pos-graduacao

Fique por dentro!
Cadastre-se como leitor, e receba os avisos da publicação de novos números por e-mail.

<http://abstracta.ifi.unicamp.br>

Abstracta

Instituto de Física
Diretor: Prof. Dr. Pascoal José Giglio Pagliuso
Diretora Associada: Profa. Dra. Mônica Alonso Cotta
Universidade Estadual de Campinas - UNICAMP
Cidade Universitária Zeferino Vaz
13083-859 - Campinas - SP - Brasil
e-mail: secdir@ifi.unicamp.br
Fone: +55 19 3521-5300

Publicação

Biblioteca do Instituto de Física Gleb Wataghin
http://portal.ifi.unicamp.br/biblioteca

Diretora Técnica: Sandra Maria Carlos Cartaxo
Coordenadora da Comissão de Biblioteca: Profa. Dra. Arlene Cristina Aguilar

Elaboração:
Maria Graciele Trevisan (Bibliotecária)
Ayres Neri da Cunha Junior
contato: infobif@ifi.unicamp.br